

# **HYDRODYNAMICS OF PAPERMAKING FIBRES IN WATER SUSPENSION**

**B. G. NORMAN, K. MOLLER, R. EK and G. G. DUFFY,**  
**Paper Technology Department, Swedish Forest Products**  
**Research Laboratory, Stockholm, Sweden**

---

**Synopsis** The rheological properties of fibre-water suspensions are of critical importance in many of the papermaking processes from stock preparation (beating, screening, fractionation, cleaning) through transport and distribution (pumping, pipe flow, headbox flow), to the actual forming process (dispersion in headbox and forming zone, dewatering).

The limitations of existing techniques for measuring velocity and turbulence as well as concentration and flocculation in pulp suspensions are discussed.

The major recent fundamental investigations of fibre suspension flow in pipes are critically reviewed within the framework of the three basic flow mechanisms (plug, mixed and turbulent flow) and the three basic study levels (empirical, network and fibre). It is concluded that the varied and complex flow phenomena exhibited by the suspensions, from plug flow through to turbulent flow, are controlled by the same variables at the fibre level: the volumetric concentration, aspect ratio and modulus of elasticity of the fibres.

Recent investigations of flocculation and turbulence are critically reviewed, and it is found that no reliable measurements of turbulence in fibre suspensions have been reported.

A new investigation of elongational pipe flow is presented.

Finally a new method for the simultaneous noncontact measurement of turbulence and flocculation is described. It is a combination of laser doppler anemometry and light reflection measurement, and offers many new possibilities in the fundamental study of pulp suspension flow.

## ***Introduction***

THE rheological properties of fibre-water suspensions are of critical importance in many of the papermaking processes from stock preparation (beating, screening, fractionation, cleaning) through transport and distribu-

*Under the chairmanship of J. Mardon*

tion (pumping, pipe flow, headbox flow), to the actual forming process (dispersion in headbox and forming zone, dewatering).

It is difficult to define or characterise a suspension of papermaking fibres in water. Three phases are present to a greater or lesser extent, solid (mainly cellulose fibres), liquid (water), and gas (air), although the presence of the latter is often ignored. These phases strongly interact with one another. Phase concentration occurs relatively easily under the action of, for example, inertial, surface tension and shear forces. A fibre suspension is also macroscopically heterogeneous in the sense that the fibres tend to agglomerate into clusters or flocs, or, at high concentrations, into continuous networks within which the local fibre concentration varies appreciably. A further complication is that no two fibres are alike in size, shape, composition or strength, so that one is forced to describe the fibres in a suspension in statistical terms. It is not surprising, therefore, that the flow properties of fibre suspensions are complex and do not conform to any of the established flow models.

The basic principles and methods used for measuring the local flow velocity and fibre concentration, as well as the local variation of these properties (turbulence and flocculation), are discussed in the first section of this paper. These subjects are introduced at this early stage since they are referred to in all the following sections.

Most investigations of the flow of fibre suspensions have been performed in pipes, many of the more recent ones by two of the authors of this paper. A summary and critical review of pipe flow investigations has been given emphasis in a special section.

Generalised Harmonic Analysis, a method used to characterise turbulence and flocculation, is described in some detail, followed by a review of significant turbulence and flocculation investigations. An investigation of the behaviour of fibre flocs during extentional pipe flow is also presented.

Finally, a new technique which can measure the local velocity and local concentration simultaneously is described. This method has the potential for investigating the inter-relationship between turbulence and flocculation, which is of primary importance, and which has not yet been determined using valid measuring methods.

Effects of the physical and chemical condition of the fibre surface are not dealt with in this paper.

### ***Measuring methods for pulp suspensions***

THE local flow velocity and the local fibre concentration are the two basic parameters that characterise a flowing pulp suspension. Since individual fibres may combine to form fibre networks with finite mechanical strength

properties, the local network strength is an important physical property. However, since no method has yet been devised for its measurement, it must be evaluated indirectly, e.g. from floc disruption under the action of known flow shear forces.

Methods for measuring local velocity, turbulence, local concentration and flocculation will now be reviewed. Their application in different investigations will be described in later sections.

**Velocity**

*Impact probes*

THIS is the most widely-used method for local velocity measurement. It employs the relationship between the local velocity and the local dynamic pressure, i.e. the difference between the total pressure and the static pressure. The total pressure can be measured using an impact probe, where a stagnation zone develops on the pressure-sensing area facing the flow. Fibres in a suspension have a tendency to accumulate on the probe tip, causing an increased disturbance of the flow and an incorrect pressure recording. This problem can be avoided by a technique introduced by Mih and Parker,<sup>(1)</sup> in which the probe tip is kept clean by the addition of flush water, as shown in Fig. 1.

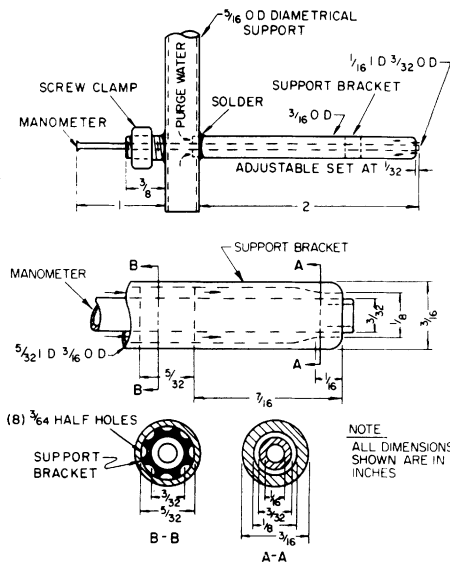


**Fig. 1**—Construction of annular purge impact tube (After Mih and Parker<sup>(1)</sup>)

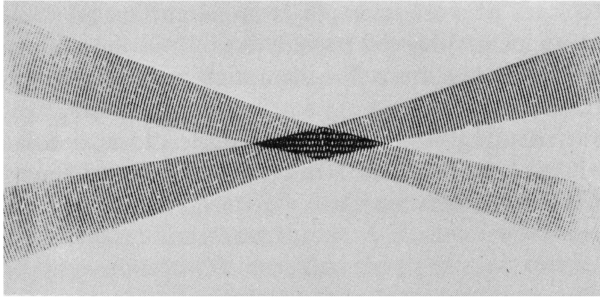


**Fig. 2**—Intersection of two laser beams

### *Laser Doppler anemometers*

Laser Doppler anemometry (LDA) is a noncontact optical method for measuring flow velocity. The individual velocities of different particles in a fluid are recorded, which means that tracer particles have to be added for measurements in pure fluids. In fibre suspensions, the fibres act as tracer particles.

An illustrative model for the understanding of LDA was presented by Rudd.<sup>(2)</sup> When two laser beams intersect at an angle of  $2\theta$  they form a pattern of plane interference fringes within the elipsoidally shaped measuring volume, as indicated in Fig. 2. The fringe separation  $\Delta x$  is calculated from

$$\Delta x = \frac{\lambda}{2 \sin \theta} \quad \dots \dots \dots (1)$$

where  $\lambda$  is the wavelength of the laser light. When a particle travels through the fringe region, light pulses are scattered at a frequency  $n$ . The particle velocity  $u$ , perpendicular to the fringes, can be calculated by the following equation

$$u = n \Delta x = \frac{n \lambda}{2 \sin \theta} \quad \dots \dots \dots (2)$$

Light emission from the measuring volume is recorded using a suitable light-detecting device, and the frequency within the 'Doppler burst' from each individual particle is evaluated electronically and multiplied by a constant to give the particle velocity according to equation (2).

There are several alternative ways of arranging the optical system, each one having a particular advantage. A system using dual beam forward detection is shown in Fig. 3.

When forward detection is impossible for geometrical reasons back scatter detection may be arranged as shown in Fig. 4. This arrangement is also

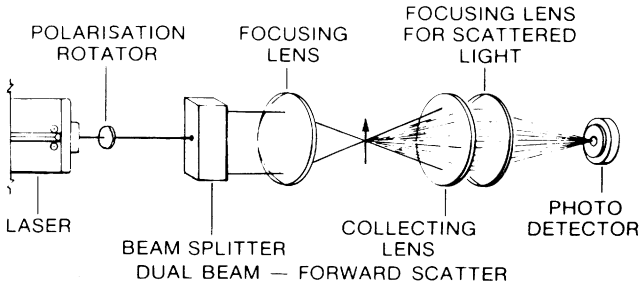


**Fig. 3**—LDA optics: dual beam-forward scatter

necessary when the dimensions of the flow channel are so large, or the fibre concentration so high, that measurements in forward detection are impossible due to excessive secondary light scattering.

A useful introduction to LDA has recently been published by Durst *et al.*<sup>(3)</sup>

LDA is being applied to fibre suspension flow at STFI and two Canadian research laboratories.<sup>(4, 5)</sup>

**Turbulence**

THE local variation in flow velocity, turbulence, is often more important than the local mean velocity in characterising a flowing pulp suspension. Relative turbulence intensity *T* is defined as the coefficient of variation *V* of local flow velocity *u*:

$$T = V(u) = \sigma(\bar{u})/\bar{u}, \quad \dots \quad (3)$$

where  $\bar{u}$  denotes mean value.

Turbulence can be further described by the turbulence spectrum, which will be discussed in a later section.

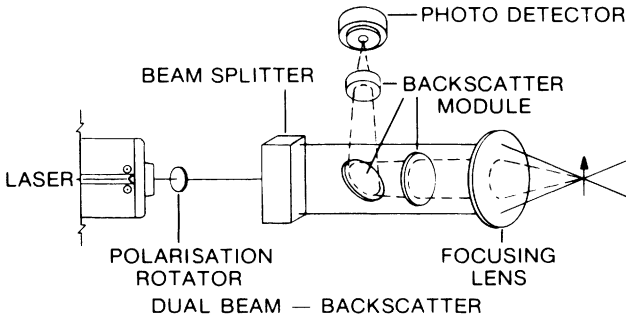


**Fig. 4**—LDA optics: dual beam-backscatter

### Hot-film anemometers

The standard method for measuring turbulence in fluids is the hot-film anemometer. A very thin metal film is mounted on a conically-shaped probe tip and heated to a constant temperature level by an electric current. Local flow across the probe tip exerts a velocity-dependent cooling effect. The current drain required to keep the temperature constant is therefore a function of the local velocity. The method can only be applied in clean fluids since scale forms an insulating layer on the metal film, thereby forcing frequent recalibration of the instrument. We have tried the instrument in a flow loop generally used for pulp flow experiments, but even after several rinsings with clean water the contamination on the probe tip was so heavy that there was a constant drift in output signal under steady flow conditions.

### Diffusion methods

Andersson<sup>(6)</sup> injected a narrow stream of dyestuff into a pulp suspension flowing in a straight channel. The distribution of dyestuff was evaluated from photographs taken in transmitted light and scanned in a microdensitometer. The turbulence intensity was calculated from the rate of dyestuff diffusion in a direction perpendicular to the mean flow direction.

Bobkowicz and Gauvin<sup>(7)</sup> injected a stream of hot fluid into a pulp suspension flowing in a pipe and measured the temperature profile downstream using a thermistor probe. The turbulence intensity was calculated from the heat diffusion characteristics.

### Impact probes

Daily *et al.*<sup>(8)</sup> and Reiner and Wahren<sup>(9)</sup> developed total head impact probes and assumed that variations in the stagnation pressure were due to fluid turbulence only. The basic equation involved (Bernoulli's equation), simplified to quasisteady conditions, states that

$$s' = 2\bar{u}u' + \left[ \frac{\rho}{2} (u')^2 + p' \right], \quad (4)$$

where  $s$  = stagnation pressure

$\rho$  = fluid density

$u$  = flow velocity

$p$  = static pressure

$\bar{u}$  = denotes mean value

' = denotes deviation from mean value.

It follows that the instantaneous velocity deviation  $u'$  is proportional to the instantaneous stagnation pressure deviation  $s'$  if the mean flow velocity is constant and if the two terms within the parentheses are negligible. The

latter is not always the case; in particular  $p'$  can be quite large if there are pressure pulses in a system. It has been shown that for isotropic turbulence there is no correlation between local velocity and local pressure.<sup>(10)</sup> If the Bernoulli equation applied there would be a strong correlation.

The theory also requires that the local stagnation pressure zone covers the whole area of the pressure sensing element. If only part of it is covered then only the corresponding fraction of the local stagnation pressure will be recorded. This fact restricts the spatial resolution, because eddies smaller than the size of the sensing area will not be fully appreciated.

Siddon<sup>(11)</sup> compared an impact probe with a hot wire anemometer, and found that the signal was attenuated for wavelengths smaller than  $4D$ , where  $D$  is the sensor diameter. Becker and Brown<sup>(12)</sup> treated the problem theoretically and found that the resolution corresponds to  $5D$ .

There appears to have been no attempt to fit a turbulence probe with a flush water system to avoid fibre stapling. Therefore no correct turbulence measurements have been performed in fibre suspensions using impact probes. This will be discussed again in a later section.

#### *Laser Doppler anemometers*

The mean local velocity and the turbulence intensity may be calculated from a large number of sampled tracer particle velocities. The accuracy can be estimated using standard statistical methods.

If a signal of velocity against time is required for evaluating the turbulence spectrum (further described in a later section), the spatial resolution is determined by the distance between the particles whose velocities are measured. This distance is partly determined by the size of the measuring volume (ellipsoidal, with typically about 0.1 mm diameter and 0.5–1 mm length), and partly by the combined capacity of the optical and electronic equipment in recording the velocity of an individual fibre. The main problem in fibre suspension measurements is the large number of tracer particles, which causes interference between different fibres within the measuring volume and disturbs the two ingoing beams as well as the scattered light between the measuring volume and the light detector. A limiting parameter is therefore the product of the penetration depth and the fibre concentration. In some cases the total penetration depth can be decreased using backscatter detection, but in this case the intensity of the scattered light is much lower than in the forward direction. As mentioned in the preceding velocity section several different optical arrangements may be used, and reference is made to e.g. Durst *et al.*<sup>(3)</sup>

Bossel<sup>(13)</sup> used an advanced optical filtration method which significantly increased the signal to noise ratio for the electronic signal. It involves incident beams with perpendicular polarisation planes and detection in two perpendicular polarisation planes. By taking the difference between the two signals, noise is in part cancelled, and the doppler burst enhanced.

It should be pointed out that mean velocity differences across the measuring volume should be an order of magnitude smaller than the fluctuating velocity component. Otherwise, even in laminar flow, particle detection in the high- and low-velocity ends of the measuring volume respectively is interpreted as turbulent fluctuations.

The geometrical resolution of an LDA is compared with that of an impact probe in a later section.

### ***Fibre concentration***

FIBRE concentration can be measured indirectly using the optical properties of the fibres. Two main optical arrangements have been used: light transmission and light reflection.

### ***Light transmission***

According to the Lambert-Beer law light transmission through a pulp suspension decreases exponentially with increasing concentration and path length through the suspension, provided the fibre concentration is low. At high concentrations the light transmission process is more complex due to secondary scattering effects. An advantage of the method is that the suspen-

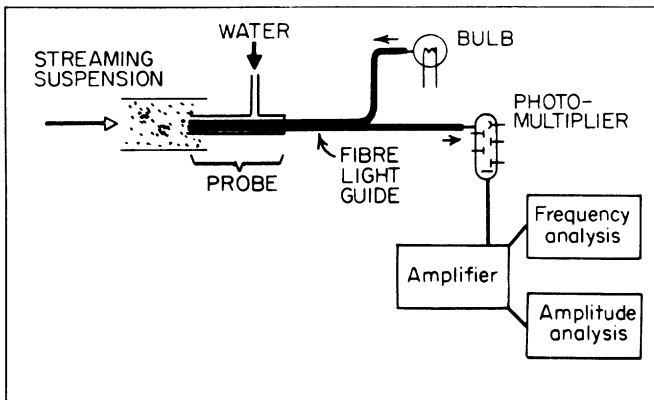


**Fig. 5**—The principle of flocculation measurement. (After Nerelius *et al.*<sup>(14)</sup>)

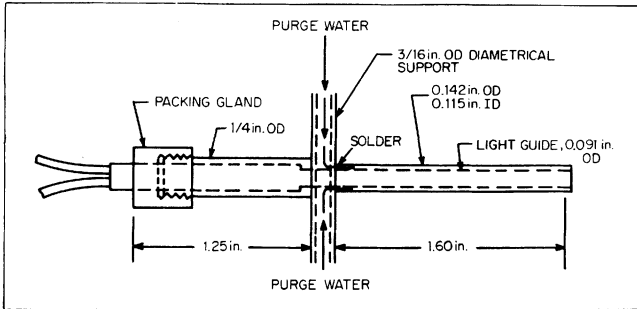


Fig. 6—Annular purge consistency probe. (After Sanders and Meyer<sup>(15)</sup>)

sion is not disturbed, but an important disadvantage is that only a weighted mean value along the entire transmission path is obtained.

*Light reflection*

Local fibre concentration has been measured using light reflection probes, the principle of which is shown in Fig. 5. A light source is placed at the end of one branch of a Y-shaped light guide, and the light is guided to the probe tip at the end of the common branch. The fibres in the suspension in front of the probe tip reflect part of the light back into the light guide, and this light is recorded by a photodetector at the end of the second branch. The probe is generally used facing upstream in a flowing suspension, and is fitted with a rinse water arrangement similar to that used on velocity probes to prevent fibre stapling. The detailed construction of a probe is shown in Fig. 6. Alternatively, the probe can be mounted with its tip flush with a flow boundary, or just outside a translucent flow boundary, in which case cleaning with rinse water is not necessary.

For a given pulp the amount of reflected light is proportional to the fibre concentration up to about 1 per cent, above which the effect of additional fibres is successively decreased due to secondary light scattering effects.<sup>(14)</sup>

**Flocculation**

A DEFINITION of flocculation, analogous to that of turbulence, was proposed by Wahren:<sup>(16)</sup>

$$P = V(c) = \sigma(c)/\bar{c}, \quad . \quad . \quad . \quad . \quad (5)$$

i.e., the relative intensity of flocculation *P* equals the coefficient of variation *V* of the local concentration *c*. Flocculation can be measured using either of the

two methods for optical concentration measurement, transmission or reflection. Photographs taken in transmitted light can be evaluated for variations in absorbance.<sup>(6)</sup> Flocculation can then be calculated if the relationship between fibre concentration and film absorbance has been determined through calibration.

In both the transmission method and the reflection method flocculation can be evaluated directly from the photo-detector signal. The standard deviation is easily measured with an RMS-meter.

The size and the shape of the measuring volume have a strong influence on the recorded flocculation. The larger the measuring volume, the more the recording of the small flocs is attenuated. In light reflection measurements the size and the shape of the measuring volume are determined both by the geometry of the optical system and by the mean fibre concentration. The influence of fibre concentration on the geometrical resolution is very complex and has to be determined experimentally (see later section Generalised Harmonic Analysis). In light transmission measurements the channel dimension is an additional geometrical factor.

The influence of the mean concentration on flocculation is very complex. On the one hand flocculation increases with increasing concentration due to mechanical entanglement of the fibres. On the other hand flocculation decreases with increasing concentration for purely statistical reasons.

*Statistical influence of concentration and measuring volume*

*Pointwise measurement* If fibres are suspended in a fluid at a volumetric concentration  $\bar{c}_v$  the local pointwise concentration is either 0 or 1, depending on whether the point of observation is situated in fluid or fibre. The variance of the concentration  $c_v$  can be calculated by integration along a scanning length  $L$  in the suspension:

$$\begin{aligned} \sigma^2(c_v) &= \frac{1}{L} \int_0^L (c_v - \bar{c}_v)^2 dl = \frac{1}{(1 - \bar{c}_v)L} \int_0^{(1 - \bar{c}_v)L} (0 - \bar{c}_v)^2 dl \\ &+ \frac{1}{\bar{c}_v L} \int_{(1 - \bar{c}_v)L}^L (1 - \bar{c}_v)^2 dl = \bar{c}_v(1 - \bar{c}_v). \end{aligned} \quad (6)$$

The coefficient of variation  $V(c_v)$  can then be calculated from

$$V(c_v) = \frac{\sigma(c_v)}{\bar{c}_v} = \sqrt{\frac{1}{\bar{c}_v} - 1}. \quad (7)$$

It is generally more convenient to express the concentration on a weight basis than on a volume basis. If the densities of the fibre and fluid are  $\rho_f$  and

$\rho_w$  respectively then the mean weight and volume fractions  $\bar{c}$  and  $\bar{c}_v$  are related by

$$\bar{c}_v = \frac{1}{1 + \frac{\rho_f}{\rho_w} \left( \frac{1}{\bar{c}} - 1 \right)} \quad \dots \quad (8)$$

Equation (8) inserted into equation (7) yields

$$V(c) = \sqrt{\frac{\rho_f}{\rho_w} \left( \frac{1}{\bar{c}} - 1 \right)} \quad \dots \quad (9)$$

Consequently,  $V(c)$  is determined only by the densities and the mean fibre concentration, and is independent of the distribution of the fibres.

Therefore, for an infinitely small measuring volume, flocculation defined as the coefficient of variation of local fibre concentration is the same for a highly-flocculated suspension as for a well-dispersed suspension provided the mean fibre concentration  $\bar{c}$  is the same. Therefore in this case,  $V(c)$  is not a useful measure of the state of flocculation in a fibre suspension. A more comprehensive description using a variance spectrum is described in a later section.

*Finite measuring volume* Since it is not possible to measure local pointwise concentration in practice, the effect of a finite measuring volume must be evaluated.

If fibres are approximated by mass points located at their centres of gravity, the simple formula for the Poisson distribution may be applied:

$$V(c) = \frac{\sigma(c)}{\bar{c}} = \frac{\sqrt{\bar{n}}}{\bar{n}} = \frac{1}{\sqrt{\bar{n}}} \quad \dots \quad (10)$$

where  $\bar{n}$  is the mean number of fibres within the measuring volume. If an approximate value of  $10^{-6}$  g is used for the single fibre weight, the mean consistency is  $\bar{c}$  per cent and the measuring volume is spherical with diameter  $D$  mm, equation (10) becomes

$$V(c) = \sqrt{3/5\pi\bar{c}D^3} \quad \dots \quad (11)$$

It is obvious from equation (11) that the magnitudes of the recorded variations in fibre concentration strongly depend on the effective size of the measuring volume. Most of the actual variations are attenuated by even the minimum size of a practical measuring volume, which is of the order of 1 mm.

*Flocculation indices*

In most flocculation investigations the results have been reported in the form of flocculation indices, which have often not been very well defined.

Comparisons between different investigations can only be made if consideration is taken of the important factors mentioned above, which is seldom possible due to lack of adequate information. Flocculation indices yield limited information and conclusions based on them should be treated with caution. A more comprehensive way of describing flocculation than merely by a single number will be described in a later section.

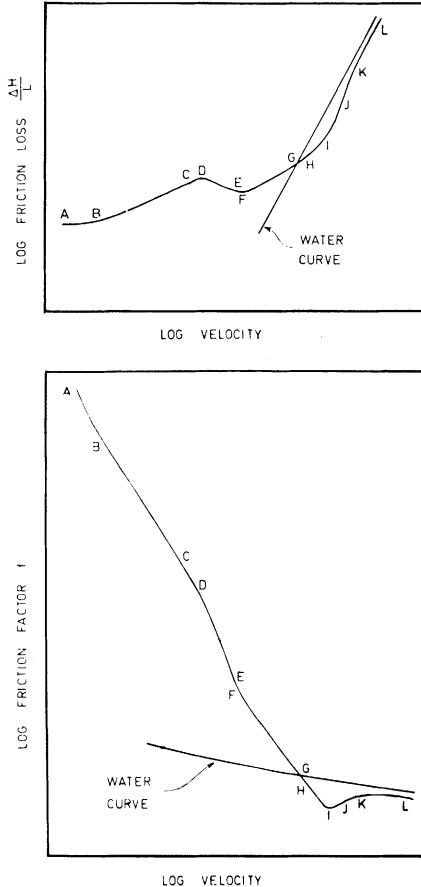


**Fig. 7**—Two common representations of pipe friction data for pulp suspensions. The relationship between Fig. 7 (a) (above) and Fig. 7 (b) (below) is given by equation (14). (After Duffy *et al.*<sup>(31)</sup>)

**The flow properties of fibre suspensions in pipes**

PRACTICALLY all studies of the flow of pulp suspensions have been performed in pipes. This is because pipe flow is experimentally relatively simple, has a sound foundation in Newtonian and non-Newtonian flow engineering, is itself one of the most important operations in the pulp and paper mill, and is relatively easy to analyse because of axial symmetry. We will therefore base our discussion and review on the characteristic pipe friction curve shown in Fig. 7, although the basic mechanisms described also apply to flow between other fixed boundaries.

**Basic concepts***Investigation level*

FIBRE suspension flow has been studied at three basic levels, although there is considerable overlap between them both historically and technically.

*The empirical level* The early studies of pulp suspension flow<sup>(17, 18)</sup> attempted to solve the problem empirically; there were few attempts to relate the flow data to the mechanisms of flow. The data were characterised in terms of a few easily-determined variables which obviously affected the friction loss, for example the flow velocity, pulp concentration, pipe diameter, pulp temperature and pulp type. This approach has only been successful for correlating data within the regime BC in Fig. 7<sup>(19-21)</sup> and will not be mentioned further here.

*The network level* This second study level resulted from observations of the basic flow mechanisms outlined below, and from a deeper understanding of the formation and properties of fibre networks.<sup>(22, 23)</sup> Here the suspension is regarded as having two components—a coherent fibre network with mechanical strength properties similar to those of viscoelastic solids, and a suspending medium with Newtonian shear properties (since it is invariably water). It was recognised that phase concentration was an important ingredient in the plug flow phenomenon and possibly also significant in the other flow regimes.

*The fibre level* The network level is only of limited use in the mixed and turbulent flow regimes and cannot explain the unusual shape of the friction curve in the plug flow range. In search of solutions to these problems it is necessary to consider the suspension in greater detail, i.e. on the fibre and floc level. Unfortunately, this third level involves a greater number of variables and is much more difficult to analyse than the network level.

There are no well-defined historical boundaries between the three study

levels but broadly speaking the empirical level was important up to about 1960, the network level began about 1955 and now appears to have nearly exhausted its possibilities, while the fibre level also began in about 1955 but has only recently gathered momentum.

### *Pipe friction characteristics*

The pipe friction curve for a pulp suspension (Fig. 7 (a)) has several distinctive features. A finite pressure gradient must be applied before the pulp begins to flow.<sup>(24)</sup> Then, as the mean flow velocity is increased the pressure gradient passes successively through maximum and minimum values and crosses the friction curve for water. At low velocities the pressure gradient for the suspension is higher than that for water while at high velocities the reverse is true, i.e. the suspension exhibits drag reduction.<sup>(25)</sup> The amount of drag reduction passes through a maximum value, and at very high velocities the pulp curve bends back towards the water curve and finally becomes parallel with it.

The effect of increasing the concentration is to move the double logarithmic curve upwards in a direction parallel to the linear water curve, while an increase in pipe diameter moves the curve downwards parallel to the pressure gradient axis.<sup>(26)</sup> In both cases the curve shape remains relatively unchanged.<sup>(18)</sup>

In several investigations<sup>(27-30)</sup> flow data have been presented on friction factor *versus* velocity diagrams, as in Fig. 7 (b). In some cases a Reynolds number calculated using the viscosity and density of water has replaced the velocity on the abscissa, but the curve form is the same. These dimensionless numbers are defined as:

$$\text{Re} = \frac{VD\rho}{\mu}, \quad \dots \quad (12)$$

$$f = \frac{2(\Delta P/L)D}{\rho V^2}, \quad \dots \quad (13)$$

where Re = Reynolds number

$f$  = friction factor

$V$  = mean flow velocity

$D$  = pipe diameter

$\mu$  = water viscosity

$\rho$  = water density

$\Delta P/L$  = longitudinal pressure gradient.

The relationship between the two types of friction diagram follows from

the definition of the friction factor:<sup>(31)</sup>

$$\frac{d \log (\Delta P/L)}{d \log V} = \frac{d \log f}{d \log V} + 2. \quad (14)$$

That is, at corresponding points the slope of the curve in Fig. 7 (a) is always greater than the slope of the curve in Fig. 7 (b) by the quantity 2. It follows that if Fig. 7 (b) is linear then so must be Fig. 7 (a) for the corresponding range of flow rates, and that if Fig. 7 (b) exhibits sharp transition points then so must Fig. 7 (a). In some cases it has been possible to represent pipe friction curves in the form of Fig. 7 (b) as three linear portions separated by sharp transition points,<sup>(27-30)</sup> presumably because of the low concentrations studied. However, this has resulted in a few anomalies in the literature<sup>(31)</sup> and can lead to misinterpretations.<sup>(32)</sup> Special care should be taken when using friction diagrams like Fig. 7 (b) because the high negative slopes in the plug flow range tend to 'wash out' important changes in Fig. 7 (a) which indicate mechanistic transitions. Furthermore, sharp transitions apparently do not occur, at least for concentrations over 1 per cent.

*Basic flow mechanisms*

Pulp suspensions exhibit three basic types of shear flow: plug flow, mixed flow and tubulent flow.

*Plug flow* Plug flow is a direct result of the tendency for the fibres in a suspension to form interlocking, coherent networks provided their concentration is over a certain minimum value.<sup>(22)</sup> Such networks have well-defined mechanical strength properties. For example, if a fibre network is subjected to a shear stress it deforms in a manner similar to that of a viscoelastic solid provided the yield value is not exceeded. If the shear yield stress,  $\tau_y$ , is exceeded then the network is destroyed, although it will reform in a new configuration when the stress is reduced to below  $\tau_y$  again.

A shear stress is applied to any fluid, including a fibre suspension, when it flows through a pipe. It is easy to show that the shear stress  $\tau$  is proportional to both the pressure loss per unit length of pipe  $\Delta P/L$  and to the distance  $r$  from the pipe axis:

$$\tau = \left(\frac{\Delta P}{L}\right) \frac{r}{2} \quad (15)$$

This stress is the greatest at the pipe wall:

$$\tau_w = \left(\frac{\Delta P}{L}\right) \frac{R}{2} \quad (16)$$

where  $R$  is the radius of the pipe and  $\tau_w$  is the wall shear stress.

Consequently, the network formed by the fibres resists destruction by the flow stresses set up in pipe flow provided  $\tau_w < \tau_y$ . However, the suspension is still able to flow for values of  $\tau_w < \tau_y$  (as opposed to a Bingham plastic fluid). This is because the stress distribution given by equation (15) causes the network to contract radially leaving a thin layer adjacent to the pipe wall in which the concentration of fibres (and hence contact and interaction between the pipe wall and the bulk of the fibre network) is reduced. This thinning process causes the suspension to begin to flow as a plug of interlocked fibres in a water matrix surrounded by a thin annulus in which all the shear flow occurs. The finite initial stress required to start flow,  $\tau_0$ , can be regarded as the yield stress of the thinned network at the pipe wall.

This annulus is always very small compared with the pipe radius so that the stress on the surface of the plug is very nearly equal to the wall shear stress. The limits of plug flow are therefore  $\tau_0 < \tau_w < \tau_y$ .

*Mixed flow* Mixed flow is a term used to describe the transition regime between plug flow and turbulent flow. An intact plug still exists in the pipe core in this regime but this is now surrounded by an annular flow area in which fibres, flocs (network fragments) and water are undergoing a complex shear flow, probably involving turbulent velocity fluctuations. A thinned or fibre-free region immediately adjacent to the pipe wall may also exist. Assuming that the shear stress on the plug surface is equal to the shear yield strength of the plug network then, combining equations (15) and (16),

$$\frac{r_p}{R} = \frac{\tau_y}{\tau_w}, \quad \dots \quad (17)$$

where  $r_p$  is the radius of the plug.

*Turbulent flow* Turbulent flow is used to describe the condition in which all the material in the pipe is in turbulent shear motion, i.e. the same as for mixed flow but without the central plug core. It may be argued that this state is never reached because the shear stress (given by equation (15)) is always zero at the pipe axis and the plug network always has a finite yield stress. But it is likely that large turbulent eddies adjacent to a small plug core deform and break the core at regular intervals. However, there is no well-defined boundary between the mixed and turbulent flow regimes.

Plug flow, mixed flow and turbulent flow are illustrated schematically in Fig. 8. These three broad classifications were introduced by Forgacs, Robertson and Mason<sup>(27, 28)</sup> and Daily and Bugliarello<sup>(29, 30, 33)</sup> in their comprehensive fundamental studies of fibre suspension flow. Some aspects of these and other early investigations were presented at the second Fundamental

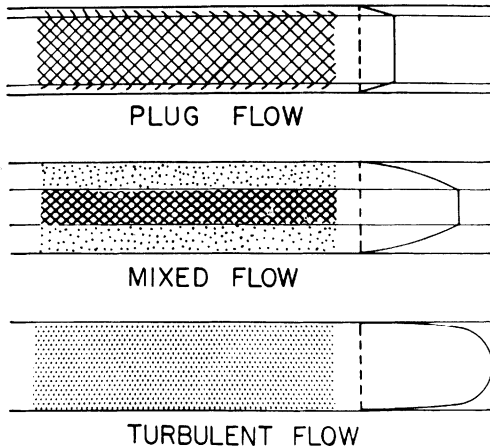


**Fig. 8**—Schematic representations of the three basic flow mechanisms of pulp suspensions in pipes. Cross-hatching represents a plug; dots represent turbulent shear flow. (After Forgacs *et al.*<sup>(28)</sup>)

Research Symposium in 1961 (see in particular <sup>(34)</sup> and <sup>(35)</sup>). It is our purpose in the next section to critically review the more fundamental investigations and results of the intervening 16 years.

### **Recent developments**

#### **Plug flow**

*Some detailed observations* As suggested by the unusual shape of the pipe friction curve within the boundaries of the plug flow regime there are, in fact, several distinctive sub-regimes or types of plug flow.<sup>(31)</sup> These have been identified partly by visual observation of the flow in clear-walled tubes,<sup>(27-29, 31)</sup> partly by a variety of experimental methods<sup>(24, 27-29, 36)</sup> and partly by theoretical considerations.<sup>(27-29, 31, 37)</sup>

The sub-regimes may be defined with reference to Fig. 7 as follows:<sup>(31)</sup>

**AB**—Plug flow where plug-wall contact predominates. The friction between the plug and the pipe wall is probably boundary friction rather than direct solid-solid friction. An annulus has not fully developed in this regime although thinned volumes exist adjacent to the wall as a result of the flocculated nature of the fibre network.

**BC**—Plug flow with combined hydrodynamic shear and plug-wall interaction. This has often been called the rolling friction regime because flocs that are

loosely held in the surface of the plug break away into the annulus and move like the rollers in a roller bearing, sandwiched between the moving plug and the stationary pipe wall. Between the rolling flocs there is an essentially fibre-free water annulus in which the flow is distributed because of the rolling flocs and the uneven surface of the plug.

DE—Plug flow with a water annulus in laminar shear. The annulus is continuous and there is no evidence of disturbances on the plug surface. Friction is purely hydrodynamic.

FH—Plug flow with a turbulent water annulus. The only superficial difference from regime DE is that a few fibres are dislodged from the network into the sheared annulus.

These sub-regimes are described in greater detail by Duffy *et al.*<sup>(31)</sup>

*Network level* In view of the above observations it is not surprising that nearly all the attempts to analyse plug flow have been conducted at the network level. Almost invariably an idealised plug flow has been assumed in which—

- (1) the annulus thickness is uniform, i.e. the plug surface is smooth;
- (2) the annulus contains water only;
- (3) the shear in the annulus is laminar and therefore obeys Newton's law of viscosity;
- (4) the annulus thickness is small compared with the plug dimensions so that the plug velocity is approximately equal to the mean flow velocity, the plug concentration is approximately equal to the suspension concentration, and the shear stress on the plug surface is approximately equal to the wall shear stress;
- (5) the velocity distribution across the annulus is linear (i.e. Couette flow).

In their considerations of plug flow Robertson and Mason,<sup>(27)</sup> Baines,<sup>(37)</sup> and Bugliarello and Daily<sup>(30, 33)</sup> concentrated on the water annulus. They derived an expression for the annulus thickness  $t$  from the above assumptions and equations (13) and (16):

$$t = \frac{\mu V}{\tau_w} = \frac{2\mu V}{(\Delta P/L)R} = \frac{\mu}{f\rho V} \quad \dots \quad (18)$$

and, as for Couette flow, defined an annulus Reynolds number  $Re'$  as:

$$Re' = \frac{Vt\rho}{\mu} = \frac{2}{f} \quad \dots \quad (19)$$

Hydrodynamic stability theory predicts that laminar Couette flow becomes unstable when  $Re' = 177$  or  $288$ , depending on the type of superimposed disturbance.<sup>(38)</sup> These values correspond well with those calculated from experimental data using equation (19) at points where other considerations

suggested a transition to turbulent flow in the annulus. The experimental values for long-fibre pulps range from 150 to 364<sup>(28, 31, 33, 37)</sup> and in general correspond to the minimum in the pipe friction curve. The annulus Reynolds number concept has proved to be useful for defining the limits of the various plug flow sub-regimes.<sup>(39, 40)</sup>

Equations (18) and (19) do not account for the role of the fibre network in the formation of the water annulus and cannot be used as flow equations, i.e. to predict the friction loss for a given flow. Baines<sup>(37)</sup> attempted to solve this problem by assuming that the plug surface stress is a constant for a given suspension and independent of flow rate. Fig. 7 (a) and assumption (4) above (a good one) indicate that this is invalid.

Analyses based on the premise that the whole plug network deforms under that action of the hydrodynamic shear stress distribution (given by equation (15))<sup>(41-43)</sup> have a sounder mechanistic basis. However, the flow equations derived by Meyer<sup>(41)</sup> were complex because they also took into account such factors as axial straining set up during flow acceleration and gravitational settling of the network. When these equations were solved using various approximations they did not fit the data of Daily and Bugliarello<sup>(29)</sup> satisfactorily.

The analysis of Moller *et al.*<sup>(42)</sup> was relatively simple. Here the deformation of the plug was assumed to be an angular one only, as shown in Fig. 9, since water is free to flow from the spacious network into the annulus. For steady

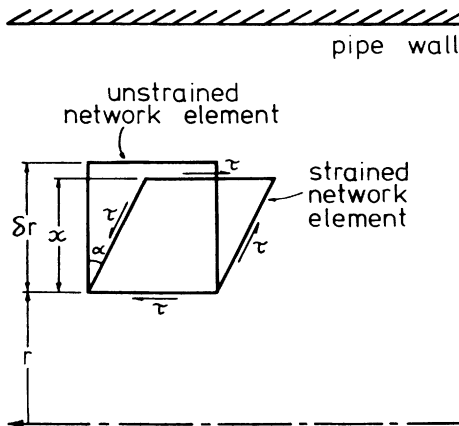


**Fig. 9**—Deformation mechanism of a fibre network element in plug flow. The unstrained configuration corresponds to zero flow. (After Moller *et al.*<sup>(42)</sup>)

state flow the strain is borne by the elastic components of the viscoelastic network, and if these are linear then

$$\tau = G\alpha, \quad \dots \quad (20)$$

where  $G$  is the network shear modulus and  $\alpha$  the shear strain.

An expression for the decrease in the radial dimension of the network element is obtained from equations (15) and (20). This is integrated over the pipe radius to yield the total decrease in radial dimension of the plug, i.e. the annulus thickness,

$$t = \frac{(\Delta P/L)^2 R^3}{24G^2} \quad \dots \quad (21)$$

Eliminating  $t$  from equations (18) and (21),

$$V = \frac{(\Delta P/L)^3 R^4}{48G^2\mu} \quad \dots \quad (22)$$

This expression allows the pressure gradient to be calculated directly from the mean flow velocity, the pipe radius, the water viscosity and the elastic shear modulus of the fibre network. The equation applies accurately to the sub-regime BC in Fig. 7, especially for the large-diameter pipes used in the pulp and paper mill.<sup>(39, 44)</sup> Values of the shear modulus may be obtained either from model pipe flow experiments, or, under certain conditions, using a special rotational viscometer.<sup>(45)</sup> A similar relationship to equation (22), expressed in terms of the wall shear stress, was derived by Babkin.<sup>(43)</sup>

Forgacs *et al.*,<sup>(28)</sup> Bugliarello and Daily,<sup>(33)</sup> and Wahren<sup>(22)</sup> have demonstrated the viscoelastic character of fibre networks using a variety of techniques. There are several other results in the literature which are consistent with both this viscoelasticity and with the network theory of plug flow. Rajj and Wahren<sup>(24)</sup> showed that the friction curve obtained during constant acceleration of the flow was higher than the curve obtained during constant deceleration for plug flow up to the minimum in the friction curve. The viscous component apparently causes a lag between the forcing function, in this case the hydrodynamic shear stress  $\tau$ , and the response of the network. The annulus thickness is therefore smaller (and consequently the pressure gradient higher) during acceleration of the flow than during deceleration. Similar responses have been observed for plug flow in a rotational viscometer<sup>(45)</sup> and in pipes<sup>(46)</sup> after the plug network is destroyed and then allowed to reform.

*Fibre level* The network models for plug flow reviewed in the previous section all predict that the pressure gradient increases with increasing flow velocity. As shown in Fig. 7 (a) this is not the case for the laminar annulus

plug flow regime between the maximum and the minimum in the pipe friction curve, i.e. the regime corresponding most closely to the assumptions made in the derivation of the models. Apparently a more detailed analysis than that afforded by the network theory is required to explain the unusual shape of the friction curve in the plug flow range.

Robertson and Mason<sup>(27)</sup> suggested that the water annulus forms as the fibre ends protruding from the plug network are deflected in the shear field of the annulus, just as grass is flattened to the earth in a wind. That is, the annulus thickness for a given suspension is a direct function of the flow velocity. On the other hand, the plug flow models reviewed above assume that the annulus develops as a result of the deforming action of the hydrodynamic shear stress on the whole plug network. That is, the annulus thickness is a direct function of the pressure gradient (equation (21)). Moller and O'Sullivan<sup>(47)</sup> proposed that the occurrence of the maximum in the friction curve could be a combined result of these two mechanisms, with the latter dominating before the maximum and the former dominating after the maximum. This idea was investigated analytically.<sup>(48)</sup> The theory predicted friction curves with the correct shape (including a maximum) and position on the co-ordinate axes. It was too complex to be used in practice but suggested that the network shear modulus  $G$ , the fibre modulus of elasticity  $E$  and the fibre dimensions are the most important network and fibre variables in the plug flow regimes. Neither this analysis nor the network models can account for the effect of pipe roughness on the friction curve,<sup>(49)</sup> which suggests that the direct plug-wall interaction associated with the rolling friction phenomenon also contributes to the occurrence of the maximum in the friction curve.

Wahren<sup>(22)</sup> has investigated the fibre-level variables which influence network properties, both theoretically and experimentally. The network shear modulus and ultimate shear strength were found to be functions of the volumetric concentration  $c_v$ , length to diameter ratio ( $l/d$ ), and modulus of elasticity  $E$  of the fibres.

*Non-Newtonian flow models* Despite the observed heterogeneity and phase separation behaviour of fibre suspensions, many investigators have applied the shear laws and correlation techniques for non-Newtonian time-independent fluids to pulp suspension flow.<sup>(33, 50-54)</sup> Some have reported success for the regime BC in Fig. 7. The reason for this is obvious if equation (22) is rewritten in terms of the wall shear stress using equation (16),

$$\tau_w = \left[ \frac{3G^2\mu}{2} \right]^{1/3} \left[ \frac{8V}{D} \right]^{1/3} \cdot \cdot \cdot \cdot \cdot \quad (23)$$

This equation has exactly the same form as the Ostwald-de-Waele power law

for a non-Newtonian time-independent fluid,

$$\tau_w = K' \left[ \frac{8V}{D} \right]^{n'} \quad (24)$$

where  $K'$  is the consistency index and  $n'$  the flow behaviour index, both constants for a given suspension. Therefore, in the plug flow regime BC, pulp suspensions are equivalent to a pseudoplastic material with  $n' = \frac{1}{3}$ . This apparent similarity is a coincidence and has no mechanistic basis. The use of the established non-Newtonian flow models and conclusions based on them must therefore be treated with caution.

### Mixed flow

*Some detailed observations* A few fibres and network fragments are dislodged from the surface of the plug in the turbulent annulus sub-regime FH in Fig. 7 but it is not until point H is reached that significant plug disruption begins.<sup>(31, 36)</sup> Point H is often close to the onset of drag reduction, point G, but can also be at a significantly higher velocity.<sup>(36)</sup> The wall shear stress (i.e. the shear yield stress of the plug network) and the mean flow velocity at point H are exponentially related to the pulp concentration.<sup>(36, 56, 57)</sup>

Mih and Parker<sup>(1)</sup> and Lee and Duffy<sup>(58)</sup> have measured velocity profiles for the mixed flow regime using special impact probes. These showed that

- (1) an intact plug of about 0.2 D still exists at I, the point of maximum drag reduction or minimum friction factor;
- (2) the stress on the plug surface, calculated from equation (17), is not a suspension property only, but has been observed to both increase<sup>(1)</sup> and decrease<sup>(59)</sup> with increasing flow rate.
- (3) the outer portions of the shear flow part of the profiles obey a semi-logarithmic velocity distribution law,

$$U^+ = A \log_e \frac{s}{R} + C, \quad (25)$$

where  $U^+$  is the reduced velocity  $= \frac{u}{\sqrt{\tau_w/\rho}}$

$s$  is the distance from the wall

$u$  is the local mean velocity

$A$  and  $C$  are constants.

However, this equation does not apply to the shear flow near the plug boundary.

*'Network' models* In the mixed flow regime an intact fibre network exists only in the plug core. The only network variable of importance here is the



that they are<sup>(62)</sup>

$$\tau'_w = \frac{\tau_w^3}{(1 - \Gamma)\tau_w^2 + \Gamma\tau_D^2} \quad (28)$$

where  $\tau'_w$  is the wall shear stress for pure water flow,  $\Gamma$  is a constant which is equal to approximately 0.35 for chemical pulps and 0.45 for groundwood pulps, and  $\tau_D$  is the wall shear stress at the onset of drag reduction, which is mainly a function of the pulp concentration.<sup>(63)</sup> This expression applies accurately to both the turbulent annulus sub-regime FH and to mixed flow up to point I in Fig. 7.<sup>(62)</sup>

*Fibre level* Fibre concentrations appear to have been too low and flow velocities too high for mixed flow to occur in the investigations of turbulent fibre suspension flow at the fibre level. However, many of the results and trends reviewed in the fibre-level section for the turbulent flow regime will also apply to the turbulent shear portions of the velocity profiles for mixed flow.

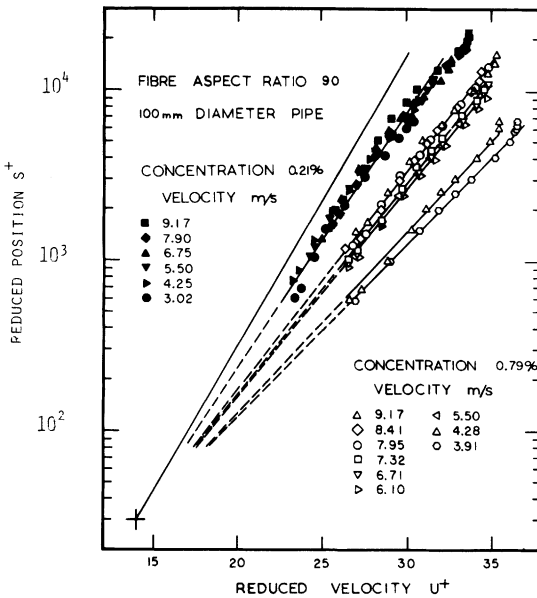


**Fig. 10**—Reduced velocity profiles for two concentrations of a pulp suspension. (After Lee and Duffy<sup>(67)</sup>)

*Turbulent flow*

*Some detailed observations* Many investigators have measured velocity profiles for turbulent fibre suspension flow using impact probes.<sup>(1, 15, 29, 30, 58, 64, 65)</sup> Those of Lee and Duffy<sup>(58)</sup> are reproduced in Fig. 10. Although there are some disagreements between the various authors, sometimes as a result of the respective ranges studied, their main findings may be summarised as follows:

- (1) The profiles obey semi-logarithmic velocity distribution laws such as equation (25) or the more general dimensionless form

$$U^+ = \frac{1}{K} \log_e S^+ + C', \quad \dots \dots \dots (29)$$

where  $S^+$  is the reduced position =  $sp \frac{\sqrt{(\tau_w/\rho)}}{\mu}$ .

For Newtonian turbulent flow  $K$  and  $C'$  are true constants, and equation (29) is known as the Universal Velocity Profile.  $K$  is called the von Kármán constant and has the value 0.4.

For turbulent fibre suspension flow  $K$  and  $C'$  in equation (29) are not universal constants. Here  $K$  is often referred to as the apparent von Kármán constant. It is a measure of the momentum transfer ability of the suspension. The higher  $K$  is, the more momentum is transferred, and the blunter the velocity profile.

- (2) In sub-regime JK in Fig. 7  $K$  increases with increasing flow rate and decreases with increasing concentration for a given type of fibre. However, at very high flow rates, in sub-regime KL in Fig. 7  $K$  varies only with the fibre concentration.<sup>(66)</sup>
- (3) All the profiles, expressed in the form of equation (29) pass through the common co-ordinates

$$U^+ = 14, \quad S^+ = 30$$

irrespective of whether they are for the sub-regime JK or the sub-regime KL.<sup>(58, 64)</sup> As a consequence of the common co-ordinates and the common slope for sub-regime KL the profiles for a given concentration lie on a common line.<sup>(1, 67)</sup>  $U^+ = 14$  and  $S^+ = 30$  are also the co-ordinates for the limit of the universal velocity profile in turbulent Newtonian flow, which suggests that the fibres in the suspension are not present in sufficient quantities to significantly modify the flow processes in the viscous sublayer ( $S^+ < 5$ ) and the buffer layer ( $5 < S^+ < 30$ ).

*'Network' models* As for mixed flow we refer to flow models which involve variables of the same scale as network variables as 'network' models, although a fibre network does not exist in turbulent flow in other than an instantaneous sense.

Mih and Parker<sup>(1)</sup> derived a flow equation for fully turbulent flow based on the observation that the friction factor was approximately constant for the sub-regime KL where the semi-logarithmic velocity profiles could be represented by a single line. This behaviour is also exhibited by Newtonian turbulent flow in rough pipes. Acting on this analogy between Newtonian flow in rough pipes and fibre suspension flow in smooth pipes, Mih and Parker<sup>(1)</sup> suggested that a suspension roughness factor  $\epsilon'$  controls the turbulent flow of a fibre suspension and that the velocity profile equation has the same form as that for Newtonian turbulent flow in a rough pipe,

$$U^+ = A \log_e \frac{S}{\epsilon'} + B = A \log_e \frac{S}{\epsilon'^{\epsilon''}}, \quad (30)$$

where the last expression is obtained by combining the constant  $B$  with  $\epsilon'$  to form a modified roughness factor  $\epsilon''$ . This equation may be integrated over the pipe radius and combined with the definition of the friction factor equation (13), to give the flow equation

$$\frac{1}{\sqrt{f}} = \frac{A}{\sqrt{8}} \left( \log_e \frac{R}{\epsilon''} - \frac{3}{2} \right). \quad (31)$$

The authors showed that  $\epsilon''$  was independent of pipe diameter and therefore a suspension property. The profile slope  $A$  and the modified roughness parameter  $\epsilon''$  must be determined from velocity profile measurements.

In a different approach Lee and Duffy<sup>(58, 66, 67)</sup> inserted the common co-ordinates given in observation (3) above into equation (29) to obtain a velocity distribution law for turbulent fibre suspension flow which involved only one profile parameter, the apparent von Kármán constant  $K$ ,

$$U^+ = \frac{1}{K} \log_e S^+ + \left[ 14 - \frac{3.4}{K} \right]. \quad (32)$$

This equation applies to both the turbulent sub-regimes, JK and KL in Fig. 7. The equation was integrated over the pipe radius, neglecting the small flows in the wall region where  $S^+ < 30$ , to give the mean flow velocity

$$V = U_* \left[ \frac{1}{K} \log_e \frac{RU_* \rho}{4\mu} + \left( 14 - \frac{4.9}{K} \right) \right], \quad (33)$$

where  $U_* = \sqrt{(\tau_w/\rho)}$ ,

or, in terms of the friction factor and Reynolds number defined by equations (13) and (12) respectively,

$$\frac{1}{\sqrt{f}} = \frac{\sqrt{8}}{K} \log_e \text{Re} \sqrt{f} + \left[ 38.6 - \frac{15.8}{K} \right]. \quad (34)$$

The constant  $K$  may be determined from velocity profile measurements, or,

for the sub-regime KL, where  $K$  is a constant for a given suspension, from laboratory experiments with a rotating disc.<sup>(66)</sup> If  $K$  is known, equation (34) can be used to calculate the pressure gradient for turbulent flow.

Equation (34) is a more useful expression for turbulent flow than equation (31), because it applies to both turbulent sub-regimes in Fig. 7, because it involves one profile parameter instead of two, and because this parameter can be determined from rotating disc experiments for the sub-regime KL.

*Fibre level* The main fibre variables affecting the flow in the turbulent drag-reducing regime have been studied for dilute suspensions of both synthetic fibres (e.g. nylon and rayon<sup>(30,68-72)</sup> and natural fibres (e.g. wood pulp and asbestos).<sup>(30,68,71)</sup> The results of these studies show that for fully-developed turbulent flow the amount of drag reduction, or deviation from Newtonian behaviour, increases with increasing

- (1) volumetric concentration,  $c_v$ ,
- (2) aspect ratio,  $(l/d)$ . Symmetric particles do not exhibit significant drag reduction,<sup>(72)</sup>
- (3) flexibility, which is inversely proportional to the modulus of elasticity  $E$  of the fibres.

An important point which was not generally recognised in these investigations is that the flow mechanism or regime plays a part in such comparisons. The effect of a particular variable may differ from one regime to the next, e.g. the maximum amount of drag reduction appears to be independent of the volumetric concentration,<sup>(61)</sup> but the flow rate at which it occurs increases with increasing concentration. Comparisons must therefore be made at corresponding points on the friction curves in Fig. 7, and not at constant velocity. However, the above results were obtained at very low concentrations and therefore high in the fully-developed turbulent regime JL, for which the stated trends are valid.

There is theoretical support for the above experimental trends. Batchelor has shown that the extensional viscosity of suspensions of rigid elongated particles is a function of the volumetric concentration and the aspect ratio, both in the case of dilute suspensions in which the particles are noninteracting<sup>(73)</sup> and in the case of suspensions of papermaking concentrations.<sup>(74)</sup>

Parallels can also be drawn with the drag-reducing properties of polymer solutions.<sup>(75)</sup> Recent evidence suggests that the mechanism of drag reduction is similar in the two systems. Asymmetric additives appear to suppress the small-scale turbulent bursts originating from instabilities in the wall region provided they are in an uncoiled configuration. These bursts normally account for much of the turbulent momentum transport near the flow



There are indications that at very high flow rates or turbulence intensities the state of flocculation in a fibre suspension approaches an equilibrium value asymptotically and that this is associated with the approach to an equilibrium flow condition. Logarithmic pipe friction curves become parallel to the water curve, i.e. the percentage drag reduction becomes constant.<sup>(61)</sup> Velocity profiles approach a common line.<sup>(1, 67)</sup> The correlation between two flocculation signals taken at the flow boundary reaches a relatively constant level.<sup>(36)</sup> The longitudinal scale of flocculation in the turbulent core approaches a constant value.<sup>(65)</sup>

Some results suggest that the fibre aggregates in a flowing suspension are anisotropic in shape. Using two flocculation probes Persinger and Meyer<sup>(65)</sup> were unable to obtain any reproducible correlation between the local concentration in the radial direction, at least for the dilute suspensions which could be tested without significant fibre stapling. The authors suggested that this could be due to the radial dimensions of the flocs being smaller than the longitudinal dimensions, which is supported by the photographic evidence of Andersson,<sup>(6)</sup> as well as by the well-known tendency for anisotropic particles to align themselves in the direction of maximum stress,<sup>(74, 78, 79)</sup> i.e. in the flow direction. This may well be related to the previously mentioned speculation of Bobkowicz and Gauvin<sup>(7)</sup> that the intensity of turbulence is higher in the radial direction than in the longitudinal direction.

Time mean concentration profiles measured by Sanders and Meyer<sup>(15)</sup> using a special light-reflectance probe indicate that the concentration increases significantly from the region near the pipe wall to the pipe axis for the turbulent flow of very dilute fibre suspensions (< 0.25 per cent) provided the flow rate is not too high. However, there are no concentration gradients in turbulent jets.<sup>(80)</sup> It is doubtful whether this effect is present in more concentrated suspensions where strong fibre interaction hampers migration. The migration of pulp particles, especially large ones, from regions of high shear gradients was first observed by Johansson and Kubát<sup>(81)</sup> and is the basis for two different separation methods used in the industry.<sup>(82-83)</sup>

#### *Mechanistic considerations for mixed and turbulent flow*

The numerous data obtained from pipe friction, velocity profile, turbulence and fibre distribution measurements in the mixed and turbulent flow regimes, which were reviewed in the previous sections, all contribute to the qualitative concept of the mechanisms of flow presented below. This concept is in general agreement with, and an extension of, the ideas of Daily and Bugliarello,<sup>(30)</sup> Vaseleski and Metzner,<sup>(68)</sup> Bobkowicz and Gauvin,<sup>(69)</sup> Kerekes and Douglas,<sup>(70)</sup> Lee and Duffy,<sup>(58)</sup> and others.

Momentum transfer is the process whereby the momentum of one fluid region is transmitted to an adjacent fluid region. The more effective the transfer, the smaller the difference in velocity between the two regions. In a flowing fibre suspension momentum appears to be transferred by three distinct mechanisms, each of which contributes a component of the total shear stress at a point in the suspension:

- (1) Viscous stress—a result of molecular interactions in the fluid phase. The important variable here is the viscosity of the fluid;
- (2) turbulent (Reynolds) stress—a result of the macroscopic motion of the fluid masses between adjacent fluid regions. The more intense the motion of such fluid masses, the more efficient the momentum transfer process. In a suspension the presence of the fibres damps the turbulence intensity by providing a force-bearing link between nearby fluid masses moving at different velocities, thereby retarding this velocity difference. The efficiency of the fibres in reducing the turbulence intensity increases with their concentration, length and flexibility (ability to follow the velocity fluctuations). These three factors can be represented by the variables  $c_v$ ,  $(l/d)$ ,  $E$ ;
- (3) fibre interlocking stress—a result of normal and frictional forces at the contact points between fibres in the suspension. The contribution to the total stress from fibre entanglement and interlocking can be expected to be a function of the same variables which affect the ultimate stress of a coherent

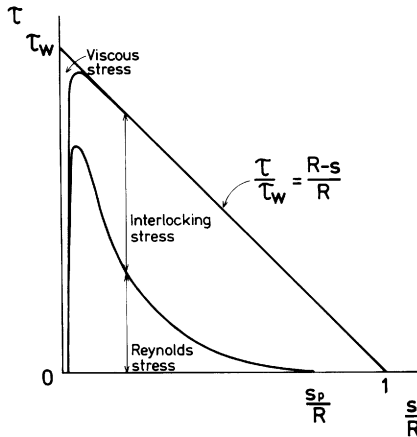


**Fig. 11**—Hypothetical distributions of the viscous, interlocking and Reynolds stress components of the total mean shear stress in a pipe for a flow rate near the point of maximum drag reduction

fibre network, i.e.  $c_v$ ,  $(l/d)$ , and  $E$  again.<sup>(22)</sup> The surface condition of the fibres (e.g. the degree of fibrillation) is probably also important. This can be represented by a surface roughness factor  $\gamma$ .

Thus the presence of the fibres affects the momentum transport in two opposing ways; on the one hand they inhibit the turbulence and thereby reduce the momentum transport, on the other hand they increase momentum transport through their own physical entanglement and interlocking. Fortunately, both of these phenomena are controlled by the same fibre variables.

The distributions of the three types of stresses over the pipe radius are represented schematically in Fig. 11 for a flow rate near I, the point of maximum drag reduction in Fig. 7. The viscous stress is important only in the relatively fibre-free sublayer and buffer layer at the pipe wall ( $S^+ < 30$ ), the Reynolds stress dominates in the highly turbulent zone adjacent to the buffer layer but then decreases rapidly with increasing distance from the wall, while the interlocking stress dominates completely further away from the wall. The interlocking stress takes all the shear stress in the plug at the pipe axis. The sum of these components, the total mean shear stress, decreases linearly from  $\tau_w$  at the pipe wall to zero at the pipe axis (see equation (15)).

If the flow rate is increased into the turbulent regime, the radial dimensions of both the plug and the viscous stress region diminish, while the Reynolds stress becomes a proportionally larger part of the total stress in the turbulent core region. At first the peak in the Reynolds stress distribution curve grows rapidly at the expense of the interlocking stress near the buffer layer. But with further increases in flow rate a state of relatively constant interlocking stress is reached (which is associated with the approach to equilibrium fibre distribution state) and the Reynolds stress region grows mostly in the radial direction.

The effect on the stress distribution shown in Fig. 11 of increasing the concentration is to increase the size of the plug and the proportion of the total stress taken by the interlocking stress.

Shear stresses break down fibre aggregates in the suspension. On the other hand the shear gradients often associated with these stresses serve to bring the fibres into new contact and therefore cause reflocculation. Thus a state of dynamic equilibrium between floc destruction and floc reformation is set up, and this equilibrium state is a function of the local stress/strain conditions.

It is possible that the Reynolds stress plays a disproportionately large role in the destruction process compared with the viscous and interlocking stresses. The Reynolds stresses shown in Fig. 11 are time-averaged values, defined by equation (35), but the instantaneous values may be considerably higher. In

addition, the variable stress will promote loosening and destruction of fibre-fibre frictional bonds. Thus, where the Reynolds stress is high, such as adjacent to the buffer layer, the fibre aggregates are disproportionately small. Conversely, where the Reynolds stress is low, such as near the plug boundary or the pipe axis, the fibre aggregates are disproportionately large.

The observed variation in the plug surface stress (calculated using plug radii obtained from velocity profiles and equation (17)) with increasing flow rate can also be explained by the disproportionate role of the Reynolds stress in breaking down fibre networks. Whether the surface stress increases or decreases with increasing flow rate depends on the shape of the stress distribution in Fig. 11. This phenomenon has also been attributed to radial concentration gradients in the suspension.

**Flow variables**

IN this review of the fundamental flow behaviour of pulp suspensions in pipes, we have attempted to classify the available information into three categories according to the scale of the variables studied or used in theoretical analyses. The empirical, network and fibre study levels also serve to give a historical perspective to developments and rank the various studies in order of increasing complexity.

We have also referred to three basic types of shear flow—plug flow, turbulent flow, and a transition between the two, called mixed flow.

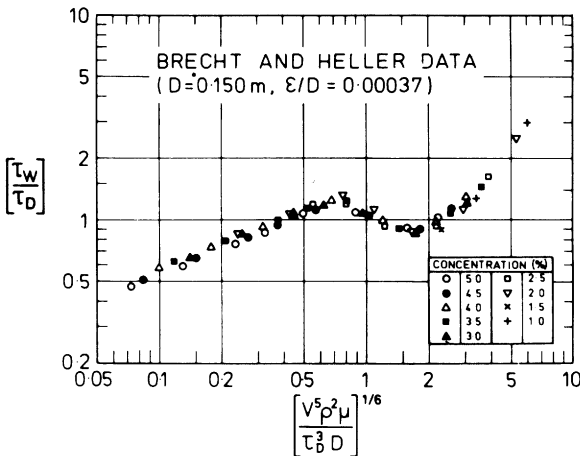


**Fig. 12**—Dimensionless correlation of the pipe friction data of Brecht and Heller<sup>(18)</sup> for a sulphite pulp flow in a 0.150 m diameter pipe with a relative roughness of 0.00037. (After Moller<sup>(63)</sup>)

Table 1 summarises the important flow variables in each of the three flow regimes for each of the three study levels, as determined by the many varied investigations reviewed above. The most surprising feature of this table is that the extremely varied flow phenomena, from plug flow through to turbulent flow, are apparently controlled by the same variables at the fibre level. The only exception is that the surface condition of the fibres is important for mixed and turbulent flow, but not for plug flow. This is a fortunate result, because the number of variables required to characterise the flow behaviour of a pulp suspension from one end of the flow spectrum to the other is kept to a minimum. It also explains why pipe friction for all the flow regimes may be correlated reasonably well using a single network parameter such as the shear yield stress, since this is a function of all the fibre-level variables  $c_v$ ,  $(l/d)$  and  $E$ .<sup>(22)</sup> Such a correlation is shown in Fig. 12 for the comprehensive friction data of Brecht and Heller.<sup>(63,84)</sup>

TABLE 1—SUMMARY OF THE IMPORTANT VARIABLES IN PULP SUSPENSION FLOW

Type of flow	Study level		
	Empirical (macroscopic variables)	Network and fluid	Fibres flocs and fluid
Plug	$C, D, V$ , etc.	$D, V, \rho, \mu, \epsilon, G, \tau_y$	$D, V, \rho, \mu, \epsilon, c_v, (l/d), E$
Mixed	$C, D, V$ , etc.	$D, V, \rho, \mu, \epsilon, \tau_y, K$	$D, V, \rho, \mu, \epsilon, c_v, (l/d), E, \gamma$
Turbulent	$C, D, V$ , etc.	$D, V, \rho, \mu, \epsilon, K$	$D, V, \rho, \mu, \epsilon, c_v, (l/d), E, \gamma$

## FLOCCULATION AND TURBULENCE

### Generalised harmonic analysis

As has been pointed out in previous sections, the state of flocculation in a flowing fibre suspension is largely determined by the interaction between fluid shear stresses (often generated by turbulence), fibres and fibre aggregates. It is a dynamic process involving deflocculation and reflocculation at various geometrical scales. Thus, since both local fibre concentration and local velocity are stochastic variables, the process must be characterised by statistical methods, which include a size distribution of eddies and fibre aggregates in the flow.

The space correlation function  $R(x)$ , correlating the instantaneous values at two points separated by a distance  $x$ , was the original method used to

extensively characterise turbulence. Simmons and Salter<sup>(85)</sup> then introduced a new method for analysing turbulence which involved filtering the signal from a hot-wire anemometer using variable high-pass and low-pass electronic filters. They measured the energy of the filtered signals and presented the results as the 'spectrum of turbulence'. Taylor<sup>(86)</sup> showed that the 'spectrum of turbulence' was in fact the Fourier transform of the space correlation function, using the mathematical theories for 'Generalised Harmonic Analysis' developed earlier by Wiener.<sup>(87)</sup> GHA applied to a stochastic signal results in the 'variance spectrum' of the signal which is defined as the distribution  $P(n)$  on different frequency ranges of the variance  $\sigma^2$  of the signal,

$$\sigma^2 = \int_0^{\infty} P(n) \, dn. \quad (36)$$

Consequently, the area below the spectrum is equal to the variance of the signal.

The term 'energy spectrum' has been used in connection with turbulence, indicating that the variance of local velocity is a measure of the turbulent energy. The term 'power spectrum' is also common, referring to the power of the voltage or current signal analysed. A more relevant term when describing e.g. local concentration variations, is the 'variance spectrum'.

For a stationary stochastic signal with a normal amplitude distribution it is convenient to transform the frequency in equation (36) to a variable which is independent of the rate of scanning (or mean flow velocity) but which will instead give information about the geometrical size of the variations. It is then obvious that the spectral density also has to be transformed in order to retain the inherent property of the variance spectrum that the area below the spectrum equals the variance of the signal.

In turbulence research the wave number  $k$  is generally used in place of the frequency  $n$ ,

$$k = \frac{2\pi n}{\bar{u}}, \quad (37)$$

where  $\bar{u}$  is the mean flow velocity at the point of measurement. The wave number expresses the number of variations per unit length rather than unit time.

In dealing with turbulence and flocculation we have found it useful<sup>(88)</sup> to transform the frequency  $n$  to the corresponding geometrical wavelength  $l$  using the relationship

$$l = \frac{\bar{u}}{n}. \quad (38)$$

It should be pointed out that this transformation is strictly valid only when the velocity  $u$  is constant, ( $=\bar{u}$ ), e.g. when scanning a sheet of paper or when

measuring on 'plug flow' of fibre suspensions. When measurements are performed in turbulent suspensions the individual floc sizes should be calculated using their individual flow velocities. Floc size spectra measured in highly turbulent flows and transformed using the mean velocity  $\bar{u}$  should be viewed with caution. It should also be pointed out that the wavelength has to be divided by a factor of two before being interpreted, e.g. as floc size, since a 'wave' consists of one 'positive' and one 'negative' floc.

The wavelength spectral density  $E(l)$  can be calculated from the frequency spectral density  $P(n)$  or the wave number spectral density  $W(k)$  using the relationships

$$E(l) = \frac{n^2}{\bar{u}} P(n) = \frac{k^2}{2\pi} W(k). \quad (39)$$

GHA has often been confused with Fourier analysis, which calls for a clarification of the fundamental difference between the two. Fourier analysis is a useful method for describing periodic functions in that it breaks down the signal into discrete frequency components. But Fourier analysis applied to a nonperiodic stochastic signal does not give meaningful results since a different set of frequency components is obtained for any two parts of the signal. On the other hand, when GHA is used the variance of the signal is presented in the form of a spectrum which includes discrete pulses for periodic components but a continuous distribution for stochastic components.

#### *The measurement of variance spectra*

There are two alternative ways of measuring the variance spectrum of a signal:

Filtering with analog bandpass filters and measuring the RMS-values of the filtered components, or

digital sampling, calculation of auto-correlation function followed by Fourier transformation.

The advantage of the former method is that the desired frequency resolution can be obtained by selecting suitable bandwidths for the individual filters. If the same relative frequency resolution is desired for the whole frequency range then filter bandwidths proportional to the corresponding centre frequency should be chosen. If  $\frac{1}{3}$ -octave filters (the bandwidths of which roughly correspond to 25 per cent of the centre frequency) are used then ten filters will cover one decade. Equipment using this principle is commercially available from a number of manufacturers and may cover a frequency range from a few Hertz up to some 100 kHz.

The digital method is particularly suitable for nonstochastic processes,

where a high frequency resolution is required in the whole frequency range, e.g. vibration analysis. When applied to stochastic signals, this type of constant-frequency resolution results in a limited frequency range (generally less than two decades) and an exaggerated frequency resolution at the high-frequency end.

### Scales

If as much of the information contained in a variance spectrum as possible is to be expressed by two parameters, then these should be the total intensity of the variations (i.e. the variance itself) and some mean scale of the variations.

Taylor<sup>(89)</sup> introduced the microscale  $\lambda$  as a measure of the smallest eddies in a turbulent flow. Although originally defined from the space correlation function  $R(x)$ , it can also be calculated from the variance spectrum using the equation

$$1/\lambda^2 = \frac{2\pi^2}{\sigma^2} \int_0^\infty \frac{E(l)}{l^2} dl. \quad (40)$$

The scale, or macroscale,  $L$  of turbulence is defined as the area below the space correlation function  $R(x)$ . In terms of the wavelength spectral density  $E(l)$  it can be expressed as

$$L = \frac{1}{4\sigma^2} \lim_{l \rightarrow \infty} [l^2 E(l)]. \quad (41)$$

The macroscale is a measure of the largest eddies or flocs in a suspension.

The scales, especially the microscale, are often strongly affected by the geometrical and/or the electronic resolution of the measuring system.

Haglund *et al.*<sup>(90)</sup> have shown that the theoretical variance spectrum of grammage in a sheet of randomly distributed fibres has a maximum at a wavelength equal to twice the diameter of the measuring area. This is due to the fact that variations of a smaller scale are attenuated because they do not cover the entire measuring area. The factor two arises from the transformation from wavelength to floc size described above.

The strong influence of the geometric and electronic resolution on the recorded variance has not always been considered in turbulence and flocculation investigations. It is therefore often impossible to draw conclusions about physical floc sizes and intensity unless the actual resolution is also taken into consideration.

An approximate estimate of the combined geometric and electronic resolution is half the wavelength at the maximum in the variance spectrum. This should be verified in the presence of a sufficient number of small-scale variations, which in the case of flocculation evaluations implies a well-dispersed suspension.

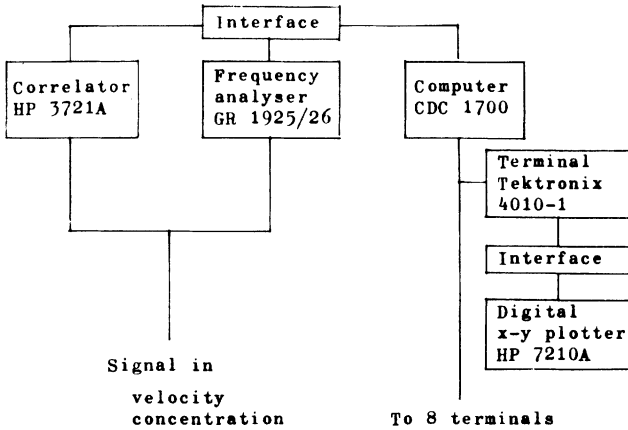


Fig. 13—The STFI signal analysis system

*The STFI signal analysis system*

The system used at STFI for the measurement of variance spectra is shown in Fig. 13. The computer is used for the storage of spectra which are to be referred to later and for transformation and normalisation purposes (e.g. calculation of the mean signal level needed for the calculation of the coefficient

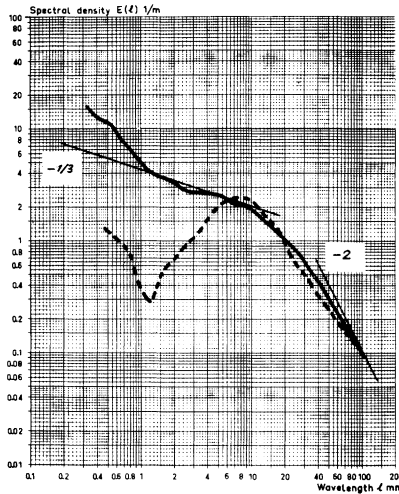


Fig. 14—Turbulence spectra: Bold curve—LDA; Broken curve—impact probe; Fine lines—theoretical slopes

of variation). A measurement can be initiated from, and the results displayed at any of the nine terminals within the institute. Including a maximum measuring time of 32 seconds, the total time from start of measurement to plotting of results is about 60 seconds. The resulting wavelength spectra are plotted on logarithmic graph paper, covering wavelengths from 0.1 mm to 200 mm (see e.g. the turbulence spectra in Fig. 14).

### ***Turbulence investigations***

#### ***Impact probe measurements***

DAILY *et al.*<sup>(8)</sup> performed the first turbulence measurements in pulp suspensions using an impact probe mounted in a pipe of 50 mm diameter. They concluded that turbulence is strongly suppressed by the addition of fibres to water. Although this result seems quite logical, and is verified by a number of other observations, it has to be pointed out that their measurements are not physically significant. A closer study of their reported turbulence spectra reveals that practically all the turbulence energy falls within a frequency range below, i.e. wavelength range above, that corresponding to the pipe diameter. Thus, they measured large-scale variations, and not what is usually understood by turbulence. The reason for this may be partly that the frequency response of their measuring system was too low and partly that there was heavy fibre build-up on the probe tip, which was not fitted with rinse-water cleaning.

Reiner and Wahren<sup>(9,91,92)</sup> used an impact probe to measure the state of turbulence in jets issuing from headboxes run with water or very dilute fibre suspensions. Their aim was to characterise the headbox, and not to investigate the effect of fibres on small-scale turbulence. The pressure-sensing element consisted of a piezo-electric disc, 3 mm in diameter. They have not reported any turbulence spectra with maxima below 10 mm wavelength, which may therefore be considered to be the spatial resolution of their instrument. Probes of the same type have since been used by several machine companies in developing new headboxes, but measurements have been performed only in pure water.

#### ***Resolution of impact probe***

The spatial resolution of an impact probe has been determined from simultaneous measurements with an LDA.

The impact probe was of the type developed by Reiner and Wahren<sup>(9)</sup> and was made by Valmet. The 3 mm diameter piezo-disc was located in the tip of a streamlined holder, 87 mm long and a maximum of 12 mm in diameter. The probe was placed a short distance from the downstream end of a straight

8 mm diameter glass tube which had a length corresponding to  $L/D = 50$  to ensure fully-developed turbulent pipe flow. The measuring volume of a DISA Mark II LDA was located in the centre of the pipe immediately before its end. The measuring volume was 0.12 mm in diameter and 0.72 mm long. An optical arrangement with forward detection (see Fig. 3) was chosen. Ordinary tap water was seeded with milk to an approximate concentration of 0.1 per cent by volume. The milk contained fat particles in the size range 0.1–20  $\mu\text{m}$ , with a probability density maximum at 3–4  $\mu\text{m}$ . Their approximate mean separation in the suspension was 0.1  $\mu\text{m}$ .

The spectra obtained at a Reynolds number of 32 000 ( $\bar{u} = 4$  m/s) with the impact probe and the LDA respectively are shown in Fig. 14. The two straight lines are theoretical slopes for random variations ( $-2$ ) and for Kolmogoroff's inertial subrange ( $-\frac{5}{3}$ ). The LDA curve follows Kolmogoroff's theory well down to wavelengths between 1 and 2 mm. Below this wavelength, noise called ambiguity broadening contributes to the spectral density. Ambiguity broadening has been discussed by e.g. George and Lumley<sup>(93)</sup> and Berman and Dunning<sup>(94)</sup>; it is caused by finite beam dimensions, velocity variations across the measuring volume and finite residence time of the scattering particles in the measuring volume. The spectrum recorded with the impact probe is strongly attenuated at wavelengths below 8 mm due to the limited spatial resolution of the probe. Therefore, this type of probe cannot be used to investigate small-scale turbulent velocity fluctuations.

### **Flocculation investigations**

As mentioned earlier most investigators have restricted themselves to measuring a less well-defined flocculation 'index', the magnitude of which is affected by channel dimensions, concentration, optical properties of the fibres and the geometry of the optical system as well as by flocculation itself. Since little information of general interest can be drawn from these investigations, they will not be considered further here. Those investigations which have produced scale information, usually *via* some form of variance spectrum, have unfortunately not included turbulence measurements (except <sup>(6)</sup>), so that it is difficult to draw general conclusions from them. Some of the recent investigations will now be reviewed.

Andersson<sup>(6)</sup> studied the flow in a 100 mm wide by 10 mm deep plexiglass channel. Flocculation was evaluated from photographs taken in transmitted light, and turbulence from the diffusion of dyestuff. It was found that the scale of flocculation was proportional to the inverse flow velocity, that the turbulence intensity was proportional to the flow velocity and that the turbulence intensity decreased with increasing concentration.

Changes in the local flocculation structure were studied with a movie camera scanning the flow at the mean velocity. Flocs were seen to break down but not to reform and there was a tendency for the flocs to be elongated in the flow direction. Floc breakdown was discussed in connection with actual measurements of floc strength, but for a complete description of the process the initial floc size distribution as well as some mechanism for floc breakdown had to be specified, which was not possible at the time.

Lafaye<sup>(95)</sup> measured variations in the light transmitted through a pulp suspension flowing in a channel  $45 \times 5$  mm in cross section. On the detection side two narrow slots in series were used to increase the optical resolution. Variance spectra were measured. Calibration tests on suspended 0.35 mm spheres resulted in a maximum recorded intensity at wavelengths around twice the sphere diameter. This result is to be expected as explained earlier. A single flocculation index was also calculated but the results were found to

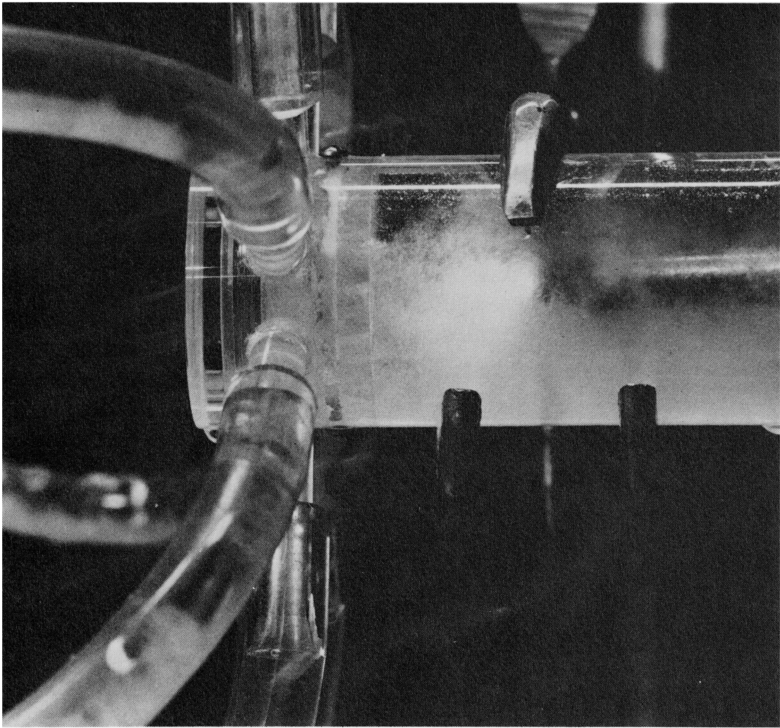


**Fig. 15**—Dispersion system, perforated plate and 40 mm diameter tube with flocculation probe inserted. (After Nerelius *et al.*<sup>(97)</sup>)

be contradictory and the use of the more comprehensive spectra was strongly recommended. Only a few preliminary results for fibre suspensions were reported.

Egelhof<sup>(96)</sup> measured variations in light transmission through a 6 mm wide channel using a 0.8 mm diameter optical aperture in the detection equipment. Further increases in the flow velocity did not affect the flocculation spectrum for Reynolds numbers above 3 000. Flocculation was found to decrease with increasing temperature and degree of beating. For a 0.3 per cent long-fibre pulp the wavelength at the maximum in the flocculation spectrum was approximately equal to twice the channel width within the range investigated (6–12 mm). This indicates that the size of the flocs was restricted by the channel dimensions and not by the flow shear field. For short-fibre pulps the flocculation maxima occurred at wavelengths smaller than the channel width.

Persinger and Meyer<sup>(65)</sup> used a light reflection probe fitted with a purge water system to study the state of flocculation across a 70 mm diameter pipe

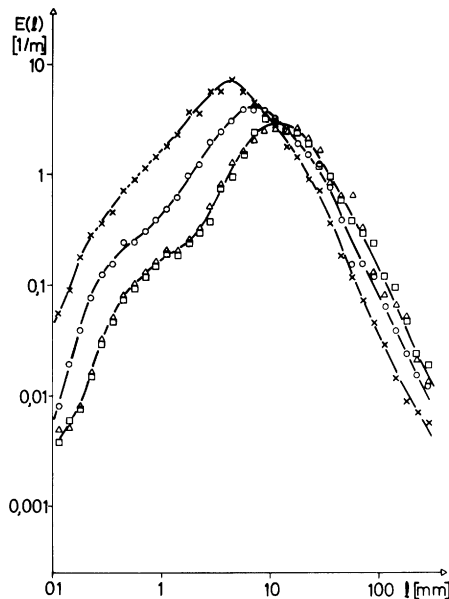


**Fig. 16**—Flocculation spectra for 0.1 per cent hardwood fibres.

Delay times: × 0.06 s      Δ 0.35 s  
                   ○ 0.17 s      □ 0.42 s

(After Nerelius *et al.*<sup>(97)</sup>)

at 1–2 m/s flow velocity and with a maximum fibre concentration of 0·1 per cent. Autocorrelation functions and the macroscale of flocculation were calculated, but the spatial resolution of the probe was not investigated. The macroscale was found to be inversely proportional to the flow velocity. Due to differences in channel dimensions and measuring technique the dominant floc sizes ( $\sim 10$  mm) differed considerably from those reported by Andersson<sup>(6)</sup> ( $\sim 1$  mm).

Nerelius *et al.*<sup>(97)</sup> measured flocculation using the light reflection probe shown in Fig. 15, which was also fitted with a purge water system. The suspension passed through a perforated plate before entering the straight reflocculation section in the 40 mm diameter pipe loop, as shown in Fig. 15. In Figs. 16 and 17, flocculation spectra measured at different distances downstream of the dispersion section are shown for 0·1 and 1·0 per cent concentration of hardwood fibres respectively. The mean flow velocity in the pipe was 0·7 m/s. It should be noted that for both concentrations steady state conditions within the smallscale floc-size range was reached between 0·17

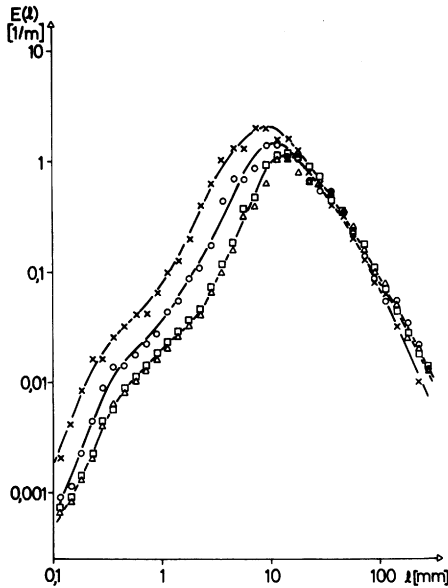


Fig. 17—Flocculation spectra for 1·0 per cent hardwood fibres.

Delay times: × 0·06 s      Δ 0·35 s  
 ○ 0·17 s              □ 0·42 s

(After Nerelius *et al.*<sup>(97)</sup>)

and 0.35 s after dispersion. For the higher concentration, steady state in the large floc-size range was reached within a few hundredths of a second.

Using the same experimental equipment Nerelius *et al.*<sup>(14)</sup> also found that flocculation is a strong function of fibre type, and that a marked increase in flocculation results when fibre concentration is increased above the sediment concentration.

### Elongational flow

THE effect on the state of flocculation of flow through cone-shaped contractions has been studied in an extensive investigation.<sup>(98)</sup>

Over 600 flocculation spectra were obtained for long- and short-fibre kraft pulps and refiner mechanical pulps. A bleached long-fibre kraft which had been Flakt-dried and reslurried was used to investigate the complete range of cone sizes. Some of the main results are summarised below.

The state of flocculation was measured using the light reflection technique described by Nerelius *et al.*<sup>(14)</sup> The probes were mounted perpendicularly to the pipe wall using the special holder shown in Fig. 18B. About 0.5 mm of the wall of the plexiglass pipe was left intact since a combination of an undisturbed wall and a short distance between probe tip and suspension is required.

The diameter of the optical area at the probe tip was 1.5 mm with the detection fibres mounted concentrically around the source fibres at the probe tip. The probe tip was smeared with silicone grease to minimise light scattering at the probe-wall interface.

Calibration of reflected light against fibre concentration was performed for the velocity ranges and probe locations of interest. These calibrations were used to evaluate flocculation from the variation in local light reflection.

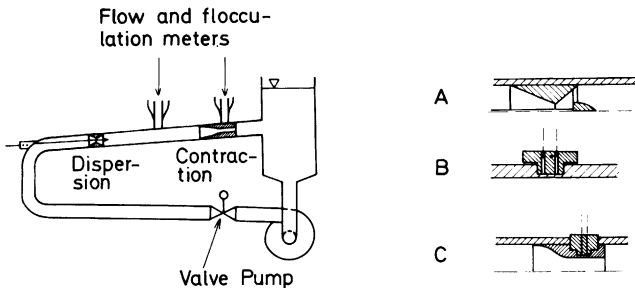


**Fig. 18**—Flow loop for the investigation of flocculation behaviour in elongational flow. Enlarged details: A. Turbulence-generating section; B. Mounting of flocculation probes; C. Mounting of contractions

If a second flocculation probe is positioned in the pipe wall at a specified distance downstream and in line with the first probe, the cross correlation function for the signals from the two probes enables the bulk velocity to be determined.<sup>(36)</sup> This method was used in this investigation.

The effect of power input into a variable speed centrifugal pump on the state of flocculation in a 20 mm diameter straight pipe downstream of the pump was studied. Two flocculation probes were placed 1.6 m (80 diameters) downstream of the pump to record flow and flocculation. The flow was throttled by a valve downstream of the measuring station to enable the pumping energy input to be varied, and the suspension returned to the pump inlet.

Three pulps were investigated over a range of flow rates from 0.5 to 3.1 m/s and at fibre concentrations ranging from 0.46 to 2.04 per cent. Power input to the pump did not affect any part of the flocculation spectrum. This result shows that an equilibrium state of flocculation is reached if the geometry of the pipe remains unchanged for 80 diameters. The result could be quite different if the state of flocculation was measured, e.g. immediately downstream of a valve at different degrees of throttling.

A small plexiglass flow loop was built to investigate changes in the state of flocculation of several types of chemical and mechanical pulp as they flowed through different conical contractions. The test section was a 2 m length of 40 mm diameter plexiglass pipe, as shown in Fig. 18. A double-conical turbulence-promoter destroyed the previous flocculation history resulting from the centrifugal pump and the valve. A slotted section, probe holder and clamps facilitated the installation of machined plexiglass cones of different sizes. The experimental arrangements for the four groups of experiments were:

- (a) a long cone which reduced the flow diameter from 40 mm to 20 mm (4:1 reduction) over a distance of 90 mm followed by a short 20 mm diameter pipe section.
- (b) three short cones which reduced the flow diameter at a constant rate over a 50 mm length to 20 (4:1), 15 (7:1) and 10 mm diameter (16:1) respectively. An 80 mm length of uniform diameter pipe followed each cone before the suspension jetted into the storage vessel.
- (c) a very short cone which reduced the flow diameter from 40 mm to 20 mm (4:1) over a distance of only 20 mm at a constant rate followed by a short 20 mm diameter pipe section.
- (d) a short cone which reduced the flow diameter to 20 mm (4:1) over a distance of 50 mm followed by a 1.01 m calming length of 20 mm diameter pipe to investigate relaxation effects.

Two flocculation probes were inserted upstream of the selected conical test section to determine the flocculation spectrum and the bulk velocity in the

pipe. One of the probes was shifted to a position downstream of the conical section (36 mm from the end of the tapered section) to obtain further flocculation spectra. For case (*d*) above, the movable probe could be positioned 36, 176, 626 and 1 014 mm downstream of the conical section.

*Bleached long-fibre kraft (dried and reslurried)* At high fibre concentrations (> 1 per cent) and low flow rates, the conditions for plug flow were favourable both in the pipe and in the throat of the conical section. For the long cone ((*a*) above), the flocculation spectra obtained upstream of the cone and at the throat (20 mm) were almost identical at wavelengths less than 30 mm (corresponding to flocs smaller than 15  $\mu$ m). However, there was a noticeable increase in the flocculation intensity at wavelengths greater than about 30 mm, indicating that the larger flocs were elongated or stretched and the plug reorganised in the conical section. At the large-scale end of the spectrum the effect was less pronounced as bulk velocity was reduced but more pronounced as fibre concentration was reduced. For the shorter 20 mm cone ((*b*) above) and the very short 20 mm cone ((*c*) above) where the elongation rate is greater, the same trends were observed in the flocculation spectra

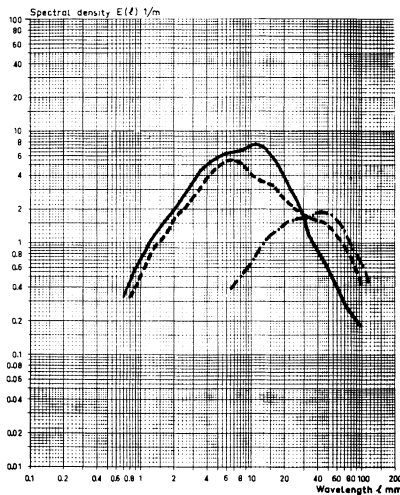


**Fig. 19**—Flocculation spectra for 0.74 per cent bleached, long-fibre kraft pulp. Pipe flow velocity 0.70 m/s.

- Approach flow
- - - After 4:1 contraction
- · - · Approach flow with 4:1 elongation

at wavelengths greater than about 30 mm. However, at the small-scale end and at the higher flow rates there was a pronounced lowering of flocculation intensity, indicating an increase in the quantity of individual fibres and very small flocs which tend to scatter the incident light from the probe and screen the larger flocs flowing below. As the flow rate was reduced the spectra at the small-scale end tended to come closer together.

Typical flocculation spectra are shown in Fig. 19. The fully drawn curve represents the state of flocculation in the approach flow in the 40 mm diameter pipe. The dashed curve is the recorded flocculation in the 20 mm diameter throat of the cone. The dashed-dotted line represents the approach flow flocculation transformed for a linear elongation of 4:1 (a shift by a factor of four along a line with slope  $-1$ ). The two broken curves can be compared for large wavelengths only since the spatial resolution of the shifted curve is limited to 30–40 mm. A comparison shows that the state of flocculation in the throat can be approximated by a simple elongation of the approach flow by an amount equal to the area reduction.

For the short 20 mm cone and subsequent calming section ((*d*) above) there was a pronounced increase in spectral density for wavelengths above about 30 mm at the position immediately following the contraction, but the spectral distribution progressively returned to its original form with increasing distance along the 1.01 m calming length. Flocs are apparently elongated and the plug reorganised to an unstable form in flowing through the cone. The instabilities are then eliminated in the calming section.

It should be noted that where transition or turbulent flow exists in the cone or calming section there will be a widening of the measured flocculation spectrum. The velocities of the individual flocs and fibres are not the same as the bulk velocity which is used to convert the frequency spectrum to the wavelength spectrum. In addition, individual fibres in turbulent motion can provide an optical screen around the flowing plug core and hence lower the overall level of spectral density over the whole wavelength range. Interpretations of flocculation spectra obtained at low fibre concentrations and at high flow rates should therefore be made with caution.

*Bleached birch sulphate (dried and reslurried)* Only one set of experiments was carried out with the short-fibre pulp using the 20 mm short cone ((*b*) above). The trends in the flocculation spectra were similar to those for the long-fibre kraft pulp but less pronounced. The difference between the flocculation spectra decreased with decreasing flow rate.

*Unbeaten and beaten, unbleached long-fibre kraft* Flocculation spectra were obtained for an unbeaten (10°SR) and beaten (21°SR) pulp flowing through the short 20 mm cone ((*b*) above). Elongation of the flocs travelling

through the conical section was obtained in both cases. There was a slight lowering of the flocculation intensity at the lower end of the wavelength spectrum probably caused by the increase in fibre debris on beating. Other differences were minor.

*Bleached refiner mechanical pulp (flash-dried and reslurried)* Flocculation spectra were obtained for a refiner mechanical pulp flowing through the short 20 mm cone ((b) above). At low flow rates through the cone, corresponding to the plug flow regime, there was no evidence of any elongation of flocs as with the chemical pulps. In fact, the flocculation spectra at the high wavelength of the spectrum from both the upstream position and the throat of the cone were in close agreement. However, at the low wavelength end of the spectrum (less than about 25 mm) there was a pronounced lowering of the spectral density in the throat of the cone, showing clearly that the acceleration effects had produced a marked increase in the amount of individual fibres and fibre fragments.

These effects were more pronounced in flocculation spectra measured at the throat of the smaller 10 mm short cone ((b) above). However, in most cases transition or turbulent flow occurred in the small diameter throat and a widening of the measured flocculation spectrum resulted. At the lowest bulk flow rate and highest fibre concentration, the spectra were almost the same at wavelengths greater than 30 mm, but the spectra obtained from the throat of the 10 mm cone at wavelengths less than 30 mm were considerably lower than the equivalent spectra obtained from the 20 mm cone above. This indicates a more intense disruption of the flocs in the smaller cone.

A further experiment was performed in the 10 mm short cone using the same mechanical pulp with the fines removed. There was a slight increase in spectral density at wavelengths greater than about 30 mm indicating floc elongation in the 10 mm cone, which was not so evident when fines were present. However, without fines there is a pronounced increase in flocculation intensity in the throat of the cone which is consistent with less fines being present. This result confirms the previously stated explanation about the effect of fines and free fibres on the recorded flocculation intensity.

In summary, these experiments have shown that strong flocs are elongated and plugs disrupted in elongational flow whereas weak flocs tend to disintegrate. Flocculation spectra obtained from a calming section following a conical contraction show that the disrupted plug returns to the original undisturbed condition. Increasing the cone angle increases the effects. The formation of a fines-rich boundary layer or a layer where individual fibres can continue to exist results in a decrease in recorded spectral density at the low-wavelength end of the spectrum.

### Combined flocculation and turbulence measurements

As has been repeatedly pointed out, turbulence and flocculation are interdependent. Turbulent shear forces deform and disrupt fibre flocs, and fibres exert a damping effect on turbulent velocity fluctuations. A realistic model of the flocculation-deflocculation process therefore inevitably requires consideration of both turbulence and flocculation. But it is not enough to characterise turbulence and flocculation separately; the correlation between the two is also important. So far no simultaneous measurements of turbulence and flocculation have been reported. In fact, as pointed out earlier, turbulence in a fibre suspension has yet to be measured correctly.

The LDA technique described in an earlier section can be modified to measure flocculation as well as turbulence. The photodetector signal contains 'Doppler bursts' (from which local velocity is evaluated) superimposed on variations of a lower frequency, which are caused by local concentration variations. If the backscatter technique shown in Fig. 4 is used then the measurements will in many respects be similar to those performed with fibre light guide probes. The main advantage compared to the light guide technique is that the measuring volume can be moved into the suspension without physically disturbing the flow.

If the measuring volume is situated well within the suspension, the amount of recorded light is the result of a combined light transmission (beams travelling to and from the measuring volume) and light reflection (within the measuring volume) process, and is governed by the equation

$$I = I_0 k_1 c e^{-k_2 c}, \quad (42)$$

where  $I$  is the recorded light intensity,

$I_0$  is the incident light intensity,

$c$  is the mean fibre concentration,

$k_1, k_2$  are constants.

Equation (42) applies when the fibres are evenly distributed. It follows that the recorded signal is affected by concentration variations in the suspension through which the ingoing and outgoing light beams pass as well as by the actual concentration variations within the measuring volume. The shorter the distance between the measuring volume and the flow boundary, the more correct the flocculation measurement.

The spatial resolution of the method has been investigated by measuring the flocculation spectrum in the centre of a 20 mm diameter pipe through which hardwood fibres at a concentration of 0.14 per cent are flowing at 1 m/s (see Fig. 20). With a measuring volume of  $0.12 \times 0.72$  mm, the spatial

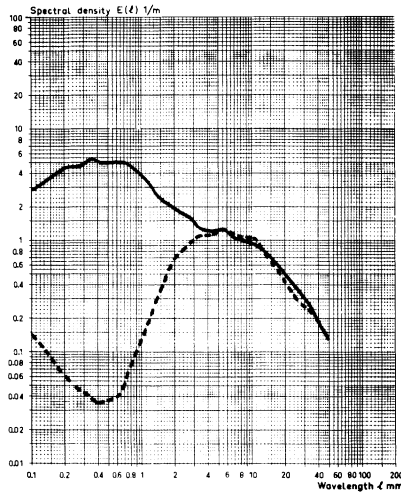


**Fig. 20**—Flocculation spectra for 0.14 per cent concentration hardwood fibres flowing with 1 m/s through a 20 mm diameter tube.

— LDA optical system  
 - - - Fibre light guide reflection probe

resolution is better than 0.5 mm. This can be compared with about 5 mm when applying the light-guide technique described in the previous section.

Combined turbulence and flocculation measurements can be performed either in back-scatter operation, in which case both velocity and concentration is evaluated from the same signal, or by a combination of forward-scatter and back-scatter. In the latter case velocity is measured using the normal forward-detection method, and concentration is measured with the back-scatter system. The requirements on the optical detector for back-scatter detection are then low, which means that a photodiode may be used.

### References

1. Mih, W. and Parker, J., *Tappi*, 1967, **50** (5), 237–246
2. Rudd, M. J., *J. Phys. E. (Sci. Inst.)*, 1969, **2** (2), 55–58
3. Durst, F., Melling, A. and Whitelaw, J. H., *Principles and practice of laser doppler anemometry* (Academic Press, London, 1976)
4. Kerekes, R., PPRIC, Montreal, Canada. Private communication
5. Lang, H., Dominion Engineering Works Ltd., Montreal, Canada. Private communication

6. Andersson, O., *Svensk Papperstidn.*, 1966, **69** (2), 23–31
7. Bobkowicz, A. J. and Gauvin, W. H., *Chem. Eng. Sci.*, 1967, **22**, 229–241
8. Daily, J. W., Bugliarello, G. and Troutman, W. W., MIT Hydrodynamics Lab. Tech. Report No. 35, 1959
9. Reiner, L. and Wahren, D., *Svensk Papperstidn.*, 1968, **71** (21), 767–773
10. Bird, R. B., Stewart, W. E. and Lightfoot, E. N., *Transport phenomena* (J. Wiley and Sons Inc., New York, 1960), 167–168
11. Siddon, T. E., *Flow: its measurement and control in science and industry, part 1* (Pittsburgh, 1971), 435–439
12. Becker, H. A. and Brown, A. P. G., *J. Fluid Mech.*, 1974, **62** (1), 85–114
13. Bossel, H. H., Hiller, W. J. and Meier, G. E. A., *J. Phys. E. (Sci. Inst.)*, 1972, **5**, 893–896.
14. Nerelius, L., Norman, B. and Wahren, D., *Tappi*, 1972, **55** (4), 574–580
15. Sanders, H. T. and Meyer, H., *Tappi*, 1971, **54** (5), 722–730
16. Wahren, D., *Svensk Papperstidn.*, 1967, **70** (21), 725–729
17. Forrest, F. and Grierson, G. A. H., *Paper Trade J.*, 1931, **92** (22), 39–41
18. Brecht, W. and Heller, H., *Tappi*, 1950, **33** (9), 14A–48A
19. Durst, R. E., Chase, A. J. and Jenness, L. C., *Tappi*, 1952, **35** (12), 529–535
20. Aktiebolaget Pumpindustri, Göteborg, Sweden, 1966, Booklet 6603 E
21. Moller, K., Duffy, G. G. and Titchener, A. L., *Appita*, 1973, **26** (4), 278–282. Errata *Appita*, 1973, **26** (5), 372
22. Wahren, D., *Svensk Papperstidn.*, 1964, **67** (13), 536–539
23. Steenberg, B., Thalén, N. and Wahren, D., *Consolidation of the paper web*, Ed. F. Bolam (Technical Section B.P. and B.M.A., London, 1966), 177–186
24. Raij, U. and Wahren, D., *Svensk Papperstidn.*, 1964, **67** (5), 186–195
25. Savins, J. G., *Trans. Soc. Petr. Engr. (AIME)*, 1964, **231** (Part 2), 203
26. Duffy, G. G., Moller, K. and Titchener, A. L., *New Zealand Engineering*, 1972, **27** (9), 273–279
27. Robertson, A. A. and Mason, S. G., *Tappi*, 1957, **40** (5), 326–334
28. Forgacs, O. L., Robertson, A. A. and Mason, S. G., *Pulp Pap. Mag. Can.*, 1958, **59** (5), 117–128
29. Daily, J. W. and Bugliarello, G., *Tappi*, 1961, **44** (7), 497–512
30. Daily, J. W. and Bugliarello, G., MIT Hydrodynamics Lab. Tech. Report No. 30, Oct. 1958
31. Duffy, G. G., Lee, P. F. W., Titchener, A. L. and Moller, K., *Appita*, 1976, **29** (5), 363–370
32. Moller, K. and Duffy, G. G., *Tappi*, 1974, **57** (7), 123
33. Bugliarello, G. and Daily, J. W., *Tappi*, 1961, **44** (12), 881–893
34. Robertson, A. A. and Mason, S. G., *Formation and structure of paper*, Ed. F. Bolam (Technical Section B.P. and B.M.A., London, 1962), 791–827
35. Wrist, P. E., *Formation and Structure of paper*, Ed. F. Bolam (Technical Section B.P. and B.M.A., London, 1962), 839–888
36. Hemström, G., Moller, K. and Norman, B., *Tappi*, 1976, **59** (8), 115–118

37. Baines, W. D., *Svensk Papperstidn.*, 1959, **62** (22), 823–828
38. Schlichting, H., *Boundary layer theory*, 1st Ed. (McGraw-Hill, New York, 1955), 314
39. Moller, K., Duffy, G. G. and Titchener, A. L., *Svensk Papperstidn.*, 1972, **75** (8), 311–316
40. Moller, K., Duffy, G. G. and Titchener, A. L., *Appita*, 1973, **26** (4), 278–372. Errata *Appita*, 1973, **26** (5), 372
41. Meyer, H., *Tappi*, 1964, **47** (2), 78–84
42. Moller, K., Duffy, G. G. and Titchener, A. L., *Svensk Papperstidn.*, 1971, **74** (24), 829–834
43. Babkin, V. A., *Mechanika Zjidkostii gaza*, 1972, No. 4, 65–71
44. Duffy, G. G., Unpublished mill-scale pipe friction data
45. Moller, K., Duffy, G. G. and Titchener, A. L., *Svensk Papperstidn.*, 1973, **76** (13), 493–499
46. Moller, K. and Norman, B., *Svensk Papperstidn.*, 1975, **78** (16), 582–587
47. Moller, K. and O'Sullivan, M. J., *Tappi*, 1974, **57** (3), 165
48. Moller, K. and O'Sullivan, M. J., Auckland University School of Engineering Report No. 93, 1973
49. Duffy, G. G., Moller, K., Lee, P. F. W. and Milne, S. W. A., *Appita*, 1974, **27** (5), 327–333
50. Guthrie, W. E., *Tappi*, 1959, **42** (3), 232–235
51. Fish, E. J., PhD dissertation, University of Melbourne, 1966
52. Serwinski, M., Kemblowski, Z., Kielbasa, J. and Iciek, J., *J. Chema Stosowana*, 1967, IV (4B), 385; 1968, V (1B), 31; 1968, V (2B), 215
53. Kurronen, S. and Wahlström, P., *Paperi ja Puu*, 1974, **56** (11), 876–890. Errata 1976, **58** (2), 94
54. Khramov, Yu. V. and Kiprianov, A. I., *Tr. Leningrad Tekhnol. Inst. Tsellyul.-Bumazh. Prom.*, 1973, No. 29, 144–149
55. Lee, P. F. W. and Duffy, G. G., Paper presented at the Appita conference, Queensland, March 1977
56. Duffy, G. G. and Titchener, A. L., *Svensk Papperstidn.*, 1975, **78** (13), 474–479
57. Duffy, G. G. and Titchener, A. L., *Tappi*, 1974, **57** (5), 162–166
58. Lee, P. F. W. and Duffy, G. G., *Appita*, 1976, **30** (3), 219–226
59. Lee, P. F. W., PhD dissertation, University of Auckland, 1975
60. Babkin, V. A., *Izv. VUZ, Lesnoi Zh*, 1974, **17** (4), 109–112
61. Duffy, G. G., PhD dissertation, University of Auckland, 1972
62. Moller, K. and Duffy, G. C., presented at the Annual Tappi Engineering Conference, Atlanta, September 1977
63. Moller, K., *Ind. Eng. Chem. Proc. Des. and Dev.*, 1976, **15** (1), 16–19
64. Seely, T., PhD dissertation, Institute of Paper Chemistry, 1968
65. Persinger, W. H. and Meyer, H., *Paperi ja Puu*, 1975, **57** (9), 563–577
66. Lee, P. F. W. and Duffy, G. G., *Tappi*, 1976, **59** (8), 119–122
67. Lee, P. F. W. and Duffy, G. G., *AIChE J.*, 1976, **22** (4), 750–753

68. Vaseleski, R. C. and Metzner, A. B., *AIChE J.*, 1974, **20** (2), 301–306
69. Bobkowicz, A. J. and Gauvin, W. H., *Can. J. Chem. Eng.*, 1965, **43**, 87–91
70. Kerekes, R. J. E. and Douglas, W. J. M., *Can. J. Chem. Eng.*, 1972, **50**, 228–231
71. Hoyt, J. W., Naval Undersea Center, Report No. NUC TP 299, 1972
72. Radin, I., Zakin, J. L. and Patterson, G. K., *Nature Phys. Sci.*, 1973, **246** (Nov. 5), 11–13
73. Batchelor, G. K., *J. Fluid Mech.*, 1970, **41**, 545
74. Batchelor, G. K., *J. Fluid Mech.*, 1971, **46**, 813–829
75. Filipsson, L. G. R., Lagerstedt, J. H. T. and Bark, F. H., Analogous behaviour of turbulent jets of dilute polymer solutions and fibre suspensions, Submitted to *Nature*, 1977
76. Bilgin, E. and Boulos, R., *Can. J. Chem. Eng.*, 1973, **51**, 405–411
77. Lee, W. K., Vaseleski, R. C. and Metzner, A. B., *AIChE J.*, 1974, **20** (1), 128–133
78. Moss, L. A. and Bryant, E. O., *Paper Trade J.*, 1938, **106** (15), 46–57
79. Baines, W. D. and Nicholl, C. I. H., *Pulp Pap. Mag. Can.*, 1956, **57** (5), 119–120
80. Walseth, D. S., PhD dissertation, Institute of Paper Chemistry, 1976
81. Johansson, B. and Kubát, J., *Svensk Papperstidn.*, 1956, **59** (23), 845–846
82. Olgård, G., *Tappi*, 1970, **53** (7), 1240–1246
83. Felsvang, K., Moller, K., Norman, B. and de Ruvo, A., To be presented at the EUCEPA conference, Vienna, October 1977
84. Moller, K., *Tappi*, 1976, **59** (8), 111–114
85. Simmons, L. F. G. and Salter, C., *Proc. Roy. Soc.*, Series A, 1938, **165**, 73–89
86. Taylor, G. I., *Proc. Roy. Soc.*, Series A, 1938, **164**, 476–490
87. Wiener, N., *Acta Mathematica*, 1930, **55**, 117–258
88. Norman, B. and Wahren, D., *Svensk Papperstidn.*, 1972, **75** (20), 807–818
89. Taylor, G. I., *Proc. Roy. Soc.*, Series A, 1935, **151**, 421–478
90. Haglund, L., Norman, B. and Wahren, D., *Svensk Papperstidn.*, 1974, **77** (10), 362–370
91. Reiner, L. and Wahren, D., *Svensk Papperstidn.*, 1971, **74** (8), 225–232
92. Reiner, L. and Wahren, D., *Svensk Papperstidn.*, 1971, **74** (9), 261–267
93. George, W. K. and Lumley, J. L., *J. Fluid Mech.*, 1973, **60** (2), 321–362
94. Berman, N. S. and Dunning, J. W., *J. Fluid Mech.*, 1973, **61** (2), 289–299
95. Lafaye, J. F., *Revue ATIP*, 1969, **23** (2), 195–206
96. Egelhof, D., *Wochenbl. f. Papierfabr.*, 1972, **100** (13), 494–499
97. Nerelius, L., Norman, B. and Wahren, D., STFI Report No. B:56, 1971 (in Swedish)
98. Duffy, G. G., Internal Report STFI, 1977

# Transcription of Discussion

## *Discussion*

---

*Dr J. Mardon* The application of laser Doppler anemometry to pulp suspensions presents some problems. The large size of the fibres relative to the seeding particles usually used can give rise to Doppler ambiguity which arises from the finite time a particle takes to cross the scattering volume. How significant is this with fibres, particularly if they are aligned in the direction of flow. If there are too many fibres it seems likely that the two beams are interrupted and they do not form a measuring volume.

*Ek* As you know a fibre has a very irregular surface and these irregularities will act as scattering particles when the fibre is passing the measuring volume. However, there will be a decreased signal to noise ratio when we have fibres instead of ideal scattering particles. This will lead to a decreased resolution.

*Mardon* What is the maximum consistency for a given fibre type that you have found usable?

*Ek* It is hard to give exact limits for the concentration, but increasing the concentration will lead to a decreased signal to noise ratio and thus decreased resolution.

*Mardon* What percentage of the time does the tracker indicate a valid signal?

*Ek* Well, the tracker—the unit which converts the Doppler frequency to an analogue voltage proportional to the velocity—sometimes cannot analyse the incoming Doppler frequency due to the low signal to noise ratio. When analysing the flow of water there is less than 5 per cent dropout and with fibre suspension it is about 10 per cent. However, it is much easier to measure mean velocities than turbulence because it is not necessary to have so many correct measurements per second in the former case. You must also plot the

*Under the chairmanship of J. Mardon*

power spectrum when you are measuring turbulence because then you can see whether the signal is acceptable or not.

*Mr W. J. McConnell* If we took two different types of fibre and measured the flow rates at the same concentration, assuming we knew the length distribution, could we then tell, using your technique, the different fibre flexibilities?

*Dr K. Moller* We cannot do that using the laser-Doppler anemometer but we could get a good idea from say the friction loss in the pipe within certain regimes. All the processes involved in pipe flow are controlled by three main fibre variables and if we know two of these then we can calculate the third inferentially.

*Dr M. B. Lyne* There must be a relationship between the depth of penetration into the pipe that is possible and the concentration of the pulp that is flowing in the pipe. Could you give us some sort of feeling how far into a large diameter pipe you could penetrate with a laser-Doppler anemometer at realistic pulp concentrations because after all, you want to look at the turbulence/flocculation relationships at realistic concentrations?

*Ek* I'll give you an approximate figure. When you have a channel 10 mm wide then the concentration could be up to approximately 1 per cent when measuring mean velocities and when measuring turbulence it should be about one tenth of that with our present equipment. But you can always compensate for this by having a more powerful laser that will increase the signal to noise ratio.

*Lyne* In practice can you penetrate beyond the annulus around a plug? Can you get into the plug itself?

*Ek* Yes.

*Mr J. B. Sisson* Have you considered being able to do this type of measurement on the papermachine?

*Ek* No, not at the moment.

*Mr J. E. Luce* With regard to the coherence spectrum: I appreciate that you said that you would reserve comment on this for some future time, but I

### *Discussion*

am struck by the larger number associated with the highest peak, 20 mm, I believe it was, and wonder whether you would care to speculate on that number being so large?

*Moller* This coherence spectrum was measured only a few days ago and we haven't had a chance to really think about it ourselves, but you must remember that the wavelength of 20 mm has to be halved so that we are really talking about variations of the order of 10 mm here. You may have noticed that there was another peak at considerably lower wavelengths than that even.

*Dr A. A. Robertson* I would like to suggest that care should be taken in interpreting the network deformation properties at different speeds. One is not always dealing with the same plug. If one increases the speed then the network one is dealing with is different in structure and properties because it is being formed at the inlet at different speeds and under different conditions. Could you comment on this?

*Moller* Originally, we did measure friction loss curves both at increasing and decreasing velocities, and while we did find some differences in the region between the maximum and minimum in the curve which could indicate differences in the structure of the plug, these were not major, so I don't think that these factors are too important, although we need to consider them of course.